Technische Universität Wien

DIPLOMARBEIT

Microdevices for Realisation of Coaxial Sheath Flows

Simulation, Fabrication and Characterisation

Ausgeführt als Student der Fakultät
Technische Physik
am Institut für

Sensor- & Aktuatorsysteme
der Fakultät
Elektrotechnik und Informationstechnik

unter der Anleitung von

Univ. Prof. Dipl.-Ing. Dr. techn. Michiel J. Vellekoop
durch

Günter Pärr

Brauhausstr. 3/2/2
2351-Wr.Neudorf
AUSTRIA

Guenter.Paerr@gmail.com

Wien, im Mai 2007

Abstract

This master thesis describes the development and design of microfluidic devices which use sheath flows to align and focus sample flows within a micro channel. The measurement of diluted particles (e.g. cells, molecules) in a MEMS device for analytical purposes for example in life science and biotechnology makes it necessary to deal with detailed problems in microfluidics. Especially when it comes to single particle detection or manipulation it is important to ensure that the particles are passing the transducer area only one by one. This requires sharp focusing techniques.

One elegant solution is to use hydrodynamic focusing in combination with sheath flows like in the work of *Jeroen H. Nieuwenhuis* [1]. This technique is used for the devices described within this thesis.
In the past various efforts have been made to characterize and describe focusing abilities in micro channels, e.g. see "Hydrodynamic Focusing in Microchannels Under Consideration of Diffusive Dispersion: Theories and Experiments" [2] or the work of *Gwo-Bin Lee* in [3]. Some published concepts were constructed in a quite complex way, requiring many fabrication steps as it can be seen in the research of *Narayan Sundararajan* in [4]. Beside this, in former articles little experimental information is given on how the shape of the formed sample flow is influenced by the related parameters.

The contribution in this thesis deals with the design and simple realization of microfluidic devices for focusing and 3D-alignment of coaxial and non-coaxial micro scale sample flows. The main design criteria is that the channel sections are all larger than $50 * 50\,\mu\text{m}^2$ (to prevent e.g. clogging effects) together with the aim to minimize the coaxial sample diameter to micrometer scale, which will allow to analyse very small particles. Within this thesis preliminary focusing limits for the tested coaxial devices could be successfully predicted and verified by experiments. They are in the range of about $2.5 \pm 1\,\mu\text{m}$ in the horizontal and $10 \pm 2\,\mu\text{m}$ in the vertical dimension. It was predicted through experiment that one of the designs will be able to give limits down to almost $1\,\mu\text{m}$ in the horizontal dimension and as the

work of my colleague Gabriel Hairer shows, this could be proved, too. For the experimental verification confocal laser microscope measurements were used. This technique allowed to prove excellent correlation of the simulated scenarios with the experimental data. It revealed detailed information on the sample flow profile and its size.

The developed devices could be used for the investigations by Gabriel Hairer which were published in [5].

To my family

Acknowledgement

Always, when somebody wants to achieve a desired goal, curiosity and enthusiasm comes up. But, there are also those moments on the long way to success and glory that are not that bright. When everything seems to be confusing and impossible, it is good in those moments to have a family you can rely on, to have friends and people taking care and helping you out.
Spending innumerable hours of empathy, work, mental support and after all love helped me to reach my desired goal and is something I do not want to forget about them.
Special thanks I am owing to the research group and the team of the ISAS department, especially to *Univ. Prof. Michiel Vellekoop* who supervised the work. Last but not least I want to thank *Dipl. Ing. (FH) Gabriel Hairer* who was coaching me, offered me support on technical issues and gave me feedback about my work and the thesis.

Vienna, May 2007

Contents

Chapter 1

Introduction

The research objective of this diploma thesis was to develop designs for hydrodynamically focusing microfluidic devices and characterize them with the related parameters. In addition to this the limiting factors to focus sample streams in such devices had to be evaluated. The main design criterion was to achieve small sample flows whereas the channels geometries are relatively large. The technological limits for fabrication and practical use with decreasing size of the device were of interest, too.

Before discussing details a brief outline about the content of this thesis is given here. To ensure a general insight into microfluidic sheath flow devices and physical aspects in fluidics Chapter 2 explains the theoretical models and their background. Chapter 3 deals with the finite element simulations which were necessary to find the right parameters to achieve the desired performance of the devices. The issues about experimental setup and practical design of the devices and their fabrication are discussed in Chapter 4. Chapter 5 is about the measurement techniques, the results of the experiments and their interpretation. The thesis is concluded with Chapter 6 . A discussion about the results and problems is presented and an outlook on future perspectives is given.

Chapter 2

Theoretical Aspects

The microdevices presented in this thesis use hydrodynamic principles to form sample fluids to a desired shape and to define their position inside a microchannel. Developing and designing such devices require mathematical models that enable to predict the behaviour of the fluids.
Before details about the design of fluidic microdevices are discussed, a background is given for the reader about the theoretical aspects. Beginning with the definition of fluids and characterising their behaviour from a classical and macroscopic point of view, limits are shown for the validity of these theories using them at smaller scales. A detailed approach in analytical models is given in the publications by *Zhigang Wu* [2] and *Gwo-Bin Lee* [3]. A more phenomenological approach is given by *James Knight* in [6].

2.1 Fluids and the Continuum Assumption

Several definitions can be found on what a fluid is and how it behaves. Some are given in [7]. One of them, [8], gives here a good starting point for further considerations refering to smaller scales:

"A fluid is a substance that deforms continuously under the application of shear (tangential) stress, no matter how small that stress may be."

It is well known that in any of the three states of matter (solid, liquid and gaseous) molecules and atoms are the elementary building blocks. Intermolecular forces as they are described by the well known *Lennard Jones* potential are responsible for their physical behaviour. To describe the physical properties on the macroscopic scale good results are achieved with using

models that are based on the continuum assumption (all quantities of interest are assumed to be defined everywhere in space and vary continuously). If the total number of particles gets small, for example if the density is low (in case of gases) or the observed volume is small (for example fluids within a micro- and nano-structure) then the continuum assumption is not valid anymore to describe such a system. More sophisticated models have to be used that include the particle motion and the particle interaction itself. The position and velocity of every single molecule of particle ensemble, together with the evolution of these parameters in time have to be considered, at least in a statistical way. This makes such models extremely complex. To avoid unnecessary investigations a lower limit for the size of systems where the continuum assumption is still valid has to be found. An approximation is given in [7] where the authors suggest length scales for fluids of 10 nm as a limit for the use of the continuum assumption. The microdevices presented in this work are systems with fluidic structures that are several times larger than the suggested limit. Therefore the continuum assumption can be assumed as acceptable. The table below allows the reader to develop a feeling for the physical characteristics of a common liquid (taken from Table 2.3 in [7]):

Property	*Liquid* H_2O
Molecular diameter	$0.3\,nm$
Number density	$2 \cdot 10^{28}\,m^{-3}$
Intermolecular spacing	$0.4\,nm$

Table 2.1: Typical Properties of H_2O

2.2 Conservation Laws and the Governing Equations

Based on the continuum assumption three primary conservation laws can be defined that are able to model thermofluid dynamic problems. Considering flows that are incompressible, isotropic, Newtonian (see further below) and belong to Fourier's law of heat conduction (heat flow is directly proportional to the temperature gradient), the conservation laws for mass, momentum and energy can be written as:

$$\frac{\partial v_i}{\partial x_i} = 0 \tag{2.1}$$

$$\rho \left(\frac{\partial v_i}{\partial t} + v_j \frac{\partial v_i}{\partial x_j} \right) = \rho F_i - \frac{\partial p}{\partial x_i} + \frac{\partial}{\partial x_i} \left[\eta \left(\frac{\partial v_i}{\partial x_j} + \frac{\partial v_j}{\partial x_i} \right) \right] \tag{2.2}$$

$$\rho c_v \left(\frac{\partial T}{\partial t} + v_i \frac{\partial T}{\partial x_i} \right) = \frac{\partial}{\partial x_i} \left(\kappa \frac{\partial T}{\partial x_i} \right) \tag{2.3}$$

Where v_i represents the flow velocities, ρ is the local density, p the pressure, F_i the body force, η the dynamic viscosity and c_v is the specific heat at a constant volume. The repeated indices indicate a summation according to the *Einstein summation convention*.
As the introduction implies thermal influences are not of interest due to the assumption of constant temperature conditions for the microdevices the equations can be further simplified to:

$$\frac{\partial v_i}{\partial x_i} = 0 \tag{2.4}$$

$$\rho \left(\frac{\partial v_i}{\partial t} + v_j \frac{\partial v_i}{\partial x_j} \right) = \rho F_i - \frac{\partial p}{\partial x_i} + \eta \frac{\partial^2 v_i}{\partial x_j^2} \tag{2.5}$$

The limit for the validity of these equations is given by the Newtonian assumption. For Newtonian fluids is the shear stress directly proportional to strain rate $\dot{\gamma}$. This behaviour breakes down when the strain rate exceeds approximately twice the molecular frequency τ:

$$\dot{\gamma} = \frac{\partial v}{\partial y} \geq \frac{2}{\tau} \tag{2.6}$$

Therefore this defines the limit for the maximum shear stress $\dot{\gamma}$ and further the maximum fluid velocity v inside microchannels.

2.3 Boundary Conditions

Obviously for solving the governing equations, initial and boundary conditions are required. For the length scales where the continuum assumption can be used, the boundary conditions are based on the argument that the velocity of the fluid shows at any point in the system always finite gradients. This implies that the fluid velocity drops to zero when reaching walls.
As the investigation about boundary conditions by *P. A. Thompson* [9] shows, the boundary conditions are valid until the shear rates get relatively high. Already at 0.3 % of the limit for the shear stress, where Newtonian behaviour breaks down, a deviation is noticeable.

2.4 Turbulence Within Microchannels

For simple geometries the *Reynolds* number Re is useful to estimate the laminar-turbulent transition for flow velocities:

$$Re = \frac{\rho \, D_h \, v}{\mu} \tag{2.7}$$

The dynamic viscosity is represented by μ. To compare fluid flows in channels and pipes of different geometries it is necessary to use the so called hydraulic diameter D_h. It represents an equivalent diameter for non-circular channel shapes, using the cross sectional area A and the wetted perimeter U as the following:

$$D_h = \frac{4 \, A}{U} \tag{2.8}$$

The transition velocity from laminar to turbulence flows depends on several parameters (e.g aspect ratio and the surface roughness). In the range of $Re = 1000$ - 2000, turbulences start to take place together with a deformation of the parabolic flow profile within the channel. For the microchannels presented in this thesis the Reynolds number is always far below 50. According to this, the flow within the channels can be considered as strictly laminar. For Reynolds numbers below $Re = 1$, the governing equations can be further simplified to the Stokes equations. The use of these equations results in better finite element simulations (reduced computing time) and in allowing to simulate hydrodynamic models with higher complexity.

2.5 Concentration and Diffusion

In biotechnology the sample fluids are for example blood cells or bacteria in a buffer fluid and are in contact with other fluids. The miscibility and the interaction (diffusion) of fluids are therefore of certain interest. For the devices that were studied in this thesis, the sample fluid consists of diluted fluorescent dye which gets manipulated and guided with sheath flows of pure de-ionized water. The use of such a diluted dye single phase system as a surrogate for biological substances allows a tremendous simplification during the experiments (e. g. atoxic, durable and stable). Beside the hydrodynamic equations, the mathematical models for the concentration and diffusion are the second group of equations that is required to describe the focusing effects within the sheath flow cells in the microdevices to full extend. Basically due

to the temperature influence particles from the sample flow collide statistically with molecules of the carrier liquid which causes them to make random movements. This results in a diffusion effect. The differential equation for diffusion is:

$$\frac{\partial c}{\partial t} = div(D \nabla C) + S \tag{2.9}$$

which is obtained from Fick's law:

$$J = -D \nabla C \tag{2.10}$$

where S represents the source or sink term of concentration and C stands for the concentration:

$$C = \frac{\partial m}{\partial V} \tag{2.11}$$

with m , the mass, and V the volume. The diffusion coefficient D depends on the temperature T, the friction factor of the fluid C_D and the Boltzmann constant k_B:

$$D = \frac{k_B T}{C_D} \tag{2.12}$$

A detailed apporach about diffusion effects can be found in the book by *Jean Berhier* [10].

2.6 Hydrodynamic Focusing Effects Inside Sheath Flow Cells

As in Chaper 1 illustrated the use of sheath flow cells offers an elegant way to combine large channel diameters without giving up the aim for small sample flow dimensions. How the principle works is discussed in the following paragraphs.
At first in Figure 2.1 a description is given of the four different types of sheath flows that are possible. Sheath flows can be single layered (a), double layered (b), coaxial (c) or non-coaxial (d). Non-coaxial (d) flow cells with integrated electrode structures can be used for impedance measurements (Coulter counter, see [11]) where coaxial (c) type is suitable for flow cytometry applications as it is illustrated by the work of *Dongeun Huh* in

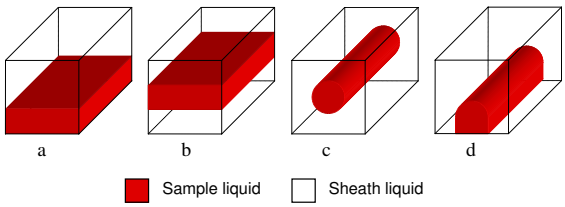

Figure 2.1: Four different types of sheath flow: single layered (a), double layered (b), coaxial (c), non-coaxial (d)

[12] and *Ren Yang* in [13]. The aim of this thesis work is to find proper

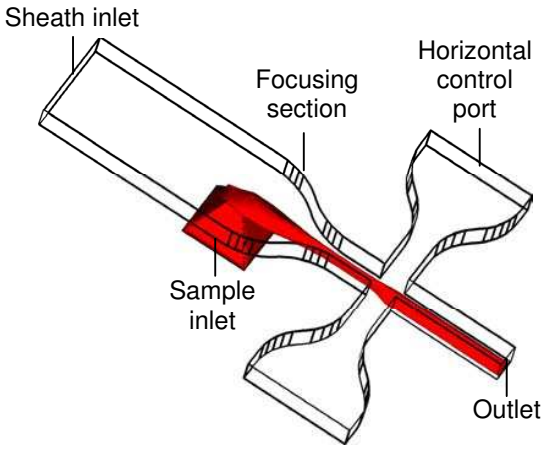

Figure 2.2: Concept for creating a non-coaxial sheath flow inside a microchannel and controlling the shape of the sample flow with the side ports.

coaxial and non-coaxial designs for sheath flow cells that are able to achieve the smallest possible sample flows within a microchannel of a certain dimension. In principle the shape of the sample flow is formed when the flow passes sections with inlets, so called ports, which are additional sources of carrier fluid. The relative pressure of the currents through the ports defines how strong the influence is on the shape. For the sake of completeness one has to mention that the use of a taper in the channel is an additional focusing technique that is used in our devices to achieve even better focusing results (see Chapter 3.1.4). All designs presented in this work are based on a cross-like structure as the non-coaxial device shown in Figure 2.2 (taken from [1]). For coaxial sheath flow cells the following principle was used. The sample flow joins through an inlet in the bottom of the device the carrier fluid and

a non-coaxial flow is created. After passing a taper another inlet in the bottom raises the sample flow and a coaxial flow is formed. In the last step two symmetric sheath flow inlets from the side focus the sample flow to even smaller dimensions. In addition to the influence on the shape, the position of the coaxial flow can be controlled by the pressures and flow velocities of the ports, too.

Chapter 3

Simulation

Prior to the beginning of this thesis non-coaxial sheath flow devices which were fabricated for detailed investigations by Jeroen Nieuwenhuis [1] were available for experiments. Based on this work und using these devices Gabriel Hairer (see [14]) pushed the knowledge even further, especially in the field of the focusing limits. These devices and results gave the starting point for the conception of the new designs. The software *FEMLAB 3.1* from *COMSOL* (see www.comsol.com, [15]) was used to carry out the numerical finite element simulations. *COMSOL-Multiphysics* allows modeling, simulating and solving physical phenomena in an interactive environment. From the so called *MODEL-LIBRARIES* the *FLUID-DYNAMICS-* and the *CONVECTION/DIFFUSION* modules were chosen to model the fluids. For simulating laminar Stokes-flows (Reynolds-number < 1, see Chapter 2) the *MEMS-MICROFLUIDCS* module was used.
The process of modeling starts with drawing the geometrical structure with the implemented CAD tool. Defining the physics of the sub-domains and setting the boundary conditions allow to generate the necessary mesh for the finite element simulation. Solving the model takes place in two steps. At first the complete fluidic problem and after this the diffusion problem is solved. The software allows to take full control over all simulation parameters, for example, correcting the automatically generated mesh, the type of solver and their parameters.
The simulations were carried out with the following assumption. Sample flow and sheath flow can be interpreted as the same liquid. It is assumed that the only difference between them is a notional concentration. The sheath flow carries 0% and the sample 100% as initial conditions. As it will be shown in the next chapter the simulation results that are based on such a model give satisfying results in comparison with experimental data (see Chapter 5).
Due to the fact that boundary conditions cause the fluid to form a hydrody-

namic flow profile the given flow rates represent always the mean values over the channel width.

3.1 Influence of Channel Geometries and Flow Rates

In this paragraph case studies are presented which illustrate the purpose and the parameters of the focusing and aligning techniques using sheath flows. The results of these simulated basic experiments allow evaluation of the design of the microfluidic devices where several sheath flow techniques are used at once. The simulations were done using a diffusion constant of $D = 1 * 10^{-9}\,\mathrm{m}^2/\mathrm{s}$. This value seems to represent the experimental sample liquid (diluted 50 mg Acridin-Orange diluted in 80 mL de-ionised water) quite well. Several different kinds of approaches were done to simulate the physical behaviour. Even if 3D simulations allow to include the dynamic of all involved parameters the influence of those does not have to be significant. After comparing equivalent simple scenarios simulated in 2D and 3D, it was concluded as not necessary for characterising the influence of the main flow parameters to investigate further into 3D simulations. Especially in Chapter 3.1.4 several assumptions of simplifications were necessary to simulate in 2D the rather complex scenario. In the critical area of interest (further details in Chapter 3.1.4) the simulated results show no significant deviation from the experimental data. Therefore the simplifications can be assumed as valid. Based on this work further analysis and 3D modeling was done by my colleage *Gabriel Hairer*.

3.1.1 Single Layered Sheath Flow - The Sample Inlet

Sheath liquid streams with a flow rate of q_{sh} and with the flow velocity v_{sh} through a straight channel section that has the cross section dimensions of $50 * 50\,\mu\mathrm{m}^2$. The sample fluid (with a certain q_{sa} and v_{sa}) is joining this flow through a rectangular inlet of the channel bottom (etched pyramid geometry of the side walls in silicon due to the lattice structure, see 5.6). The ascending height h_x of the non-coaxial sample flow in relation to the channel height is of interest. The varied parameters in the simulations were the ratio of q_{sh}/q_{sa}, the v_{sh}/v_{sa} and the absolute value of q_{sh}. The velocity ratio was defined by the length of the sample inlet (channel width was kept fixed at $50\,\mu\mathrm{m}$). One of the 2D simulations together with all variables shows Figure 3.1. In the simulation the varying concentration was measured across the channel. The measurements were taken at position A, around $50\,\mu\mathrm{m}$ after the rear sample

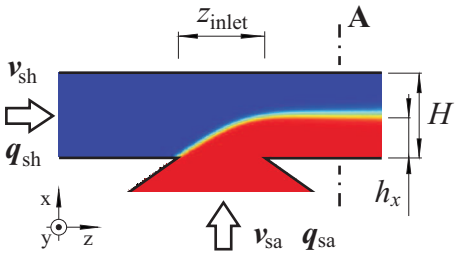

Figure 3.1: Lateral 2D simulation of the sample inlet ($q_{sh} = 1\,\mu\mathrm{L}/min$ and $q_{sh}/q_{sa} = 1$). The measurements, like in Fig. 3.2 were taken at position A.

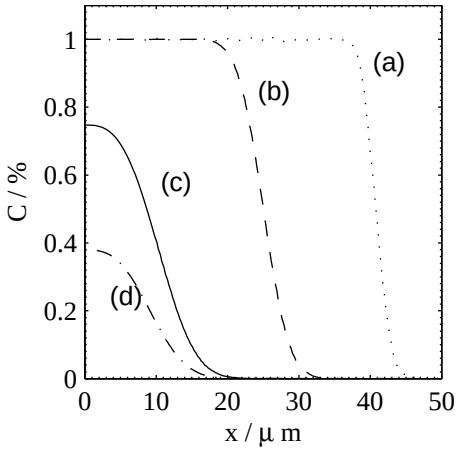

Figure 3.2: Cross section plots of the varying concentration at position A with flow ratios of $q_{sh}/q_{sa} = (a)\,0.1, (b)\,1, (c)\,10, (d)\,25$ and $q_{sh} = 1\,\mu\mathrm{L}/min$

inlet edge. Several simulations were done, each one with different sample inlet geometry (sample inlet length varied from 25 % to 200 % of 50 μm channel height) and a varied flow rate $q_{sh} = 0.1, 1, 10\,\mu\,L/min$). For each specific q_{sh} simulations the ratio of the flow rates q_{sh}/q_{sa} were varied (between 0.1 and 30 μL/min). Each simulation gave an array of curves showing how the concentration varies across the channel height (Figure 3.2). The height h_x was then determined by the distance from the channel bottom to the point where the concentration drops to 50 % of the maximum. As an example the simulated heights h_x for a sheath flow rate of $1\,\mu\,L/min$ is represented in Figure 3.3. It shows how high the sample flow ascends and how it depends on the different parameters. The simulations indicate that h_x depends also on the absolute value of the flow rates. That means that increasing the ratio of the flow rate q_{sh} results in a decreased sample height (downward shift of the curves). Therefore higher absolute flow rates (around 1 to $10\mu\,L/min$) seem to improve the focusing quality (minimal sample height at lowest flow rate ratio). Also the aspect ratio of the inlet (rectangular or square) influenced the results slightly. At lower flow rates this effect is more noticeable like it is shown by in Figure 3.4. The effect of the inlet dimension can be seen as a splitting up of the curves at higher flow ratios. Large lateral aspect ratios in the 2D-simulations show that the sheath liquid tends to flow into the sample inlet and causes noticeable deformation of the sample flow in this area (see Figure 3.5 and the confocal fluorescent images, Figure 5.9, too). On

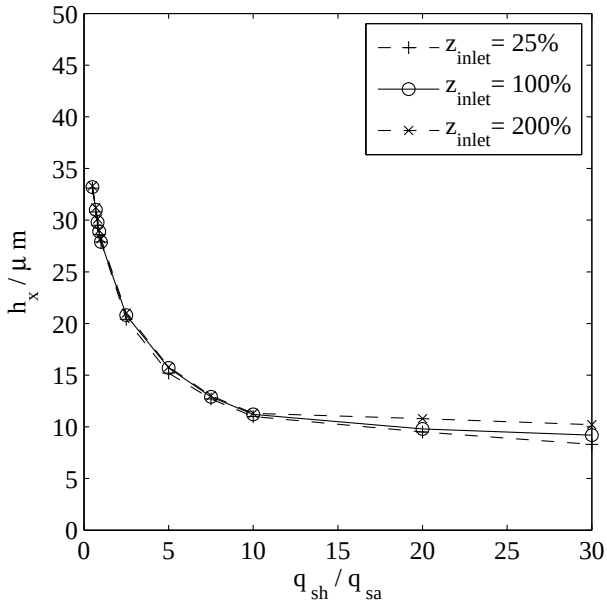

Figure 3.3: The height of the sample flow h_x as a function of the flow ratio q_{sh}/q_{sa} at a flow rate of $q_{sh} = 1\,\mu$L/min and a lateral length of the inlet z_{inlet} varying between 25 %, 100 % and 200 % of the channel height $H = 50\,\mu$m

the other hand decreasing the dimensions of the sample inlet to a narrow transversal slit results in a flow similar to those from a jet. This principle is illustrated in Figure 3.6. Only 3D simulations of this scenario can give accurate results. Theoretically with this principle a double layered coaxial sheath flow can be generated. The limiting fact would be the Reynolds number which can become significantly high. For the design of such bottom inlets a square geometry of the same dimensions as the channel itself seems to be a good choice to avoid additional diffusion, higher Reynolds numbers and small inlets.

3.1.2 Double Layered Sheath Flow - The Uplifting Port

To avoid the interesting but rather complicated lithographic fabrication of slopes in the vertical plane along the microchannel together with a nozzle like in the article by *R. Yang* [13] or a chimney-like structure like in [16] by *A. Wolff* and to have control over the position and shape of the sample flow an additional inlet in the bottom, like in [17], is used to realise a coaxial sheath flow. A single layered sheath flow (q,v) enters, with a sample flow height of h_{sa}, a $50 * 50\,\mu$m^2 straight channel section and gets raised up by an uplifting sheath flow (q_{li}, v_{li}) which is flowing through an inlet in the bottom

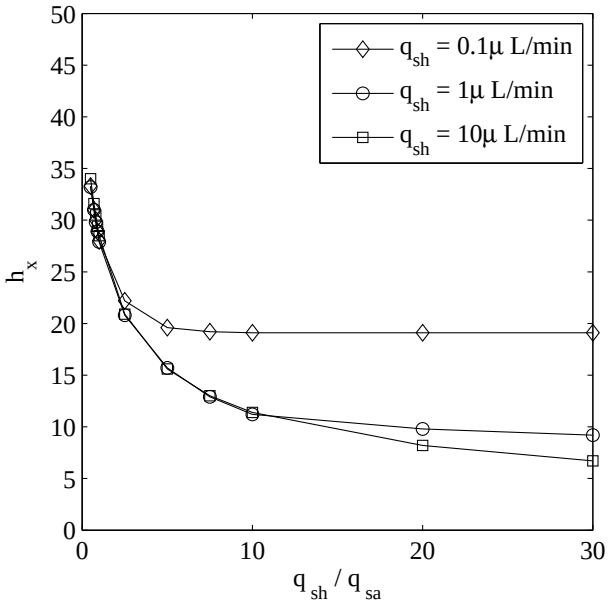

Figure 3.4: The influence of the absolute q_{sh}-value on h_x as a function at a fixed lateral length of the inlet x_{inlet} of 100 % of the channel height $H = 50\,\mu$m

of the channel, the so called up-lifting port (same dimensions). The uplifted height of the sample flow centre and its thickness w_x after passing the port is of interest and was measured. The varied parameters are first, the height of the sample flow h_{sa} at the entrance (varied between 25%, 50% and 75% of the channel height) and second the ratio of the flow rates q/q_{li}. Figure 3.7 shows a 2D-simulation with all variables and dimensions. Concentration measurements reveal figures like in Figure 3.8. The position of the sample flow h_x is determined by the position of the concentration-peak, the width w_x is defined by the values on the abscissa where the concentration drops below 50%. Drawing for a certain q the position and the width w_x of the sample flow over the flow rate ratio q_{li}, v_{li} gives graphs like Figure 3.9 and Figure 3.10 (h_{sa} is the free parameter).
Comparing such graphs with those of different absolute flow rates show that higher flow rates result in smaller focused sample flows. Combining these conclusions together with the diagrams and the information of the last paragraph allows now to characterize microdevices which combine these two principles. These results allow now to determine, at least for the vertical plane, the achievable sample flow position and width in a combination of a sample flow inlet together with an uplifting inlet in the bottom of a channel with certain flow rates and velocities.

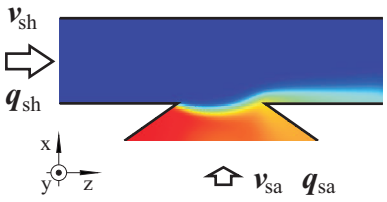

Figure 3.5: Noticeable back flow into the sample inlet with increased flow ratio of $q_{sh}/q_{sa} = 25$ at $q_{sh} = 1\,\mu\text{L}/min$

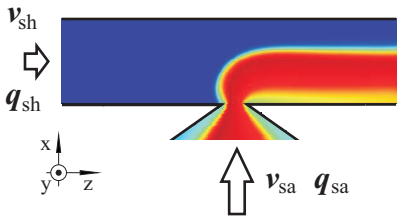

Figure 3.6: Coaxial-like sheath flow at a low flow ratio of $q_{sh}/q_{sa} = 0.8$ and $q_{sh} = 10\,\mu\text{L}/min$

3.1.3 Symmetric Double Layered Sheath Flow - The Side Ports

To achieve in a simple way horizontally plane and symmetrically focused sample flows the following principle is quite common. Sample liquid is flowing (q_{sa}, v_{sa}) in a straight channel ($50*50\,\mu\text{m}^2$) that passes an intersection. From the so called side ports flows sheath liquid (q_{po}, v_{po}) symmetrically (to achieve a centered flow) toward the sample flow. The mass conservation principle forces now the sample flow to reduce its lateral width accordingly to the ratio of q_{po}/q_{sa}. An illustration is given in Figure 3.11 and the concentration along the channel cross section is shown in Figure 3.12.
In the simulations the flow ratio of q_{sa}/q_{po} was varied from $0,01$ to 100 for flow rates between $0,1-20\,\mu\text{L}/\text{min}$. Figure 3.13 shows the influence of q_{sa}/q_{po} and q_{sa} on the achievable sample width. It shows that in the simulations sample widths of less than $1\,\mu\text{m}$ can be achieved in a single focusing step. But such results require a flow rate ratio of around 40 and more. Practically, this would mean a tremendous stress inside the channels of the microdevice which would likely result in damaging the device. Therefore it can not be assumed the possibility to achieve a sample width less than 5% by only a simple focusing step. As it will be discussed later this is the reason why a combination of several focusing techniques has to be used to reach even smaller limits.

3.1.4 The Taper

Considering laminar flows inside a microchannel allow the use of a taper (decreasing channel width) to reduce the width of a sample flow, too. The density of the streamlines inside a laminar flow is therefore strictly proportional to the channel width. Considering the aspects of simplification discussed in

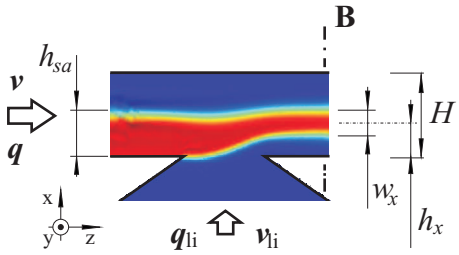

Figure 3.7: Lateral 2D simulation of the uplifting port. The measurements were taken at position B ($q/q_{li} = 5$, $q = 1\,\mu\mathrm{L}/min$).

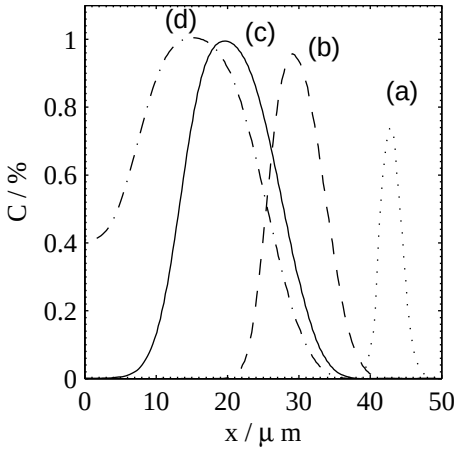

Figure 3.8: Varying concentration influenced by the uplifting inlet at position B and $q = 1\,\mu\mathrm{L}/min$: q/q_{li} =(a) 0.1, (b) 1, (c) 5 and (d) 25

Chapter 3.1 the following 2D model was used. Assuming a setup as illustrated in Figure 3.14 which shows a top view of a taper where a sheath flow (q_{sh}, v) and a sample flow (q_{sa}, v) enter a channel from the left. The channel width w gets decreased to a final width w'. The lateral dimension of the sample inlet w_{sa} gets projected to the size w'_{sa}. The sample size is reduced by the same factor as the channel changes its dimensions from w_{sa} to w'_{sa}. Allowing diffusion of the sample flow results in slightly different behaviour, especially when it comes to low ratios of q_{sh}/q_{sa} and low absolute flow rates. An illustration is given in Figure 3.15 showing a sequence of 2D simulations with varying parameter q_{sh}.
Measurements of the concentration across the channel show the minimal ratio of the flow rates where the sample width gets compressed by the same factor like the channel decreases its size (Figure 3.16). Flow ratios higher than $q_{po}/q_{sa} = 5$ give the best performance of the taper.

3.2 Design Considerations

Based on the results of the previous paragraphs it can be estimated how these focusing techniques have to be used and the microchannels have to be designed to achieve sample flow dimensions that are desired. To achieve a coaxial sheath flow within such a microdevice a certain combination of focusing and aligning techniques has to be used. The aim is to produce a sample flow inside a microchannel that is only in contact with the sheath

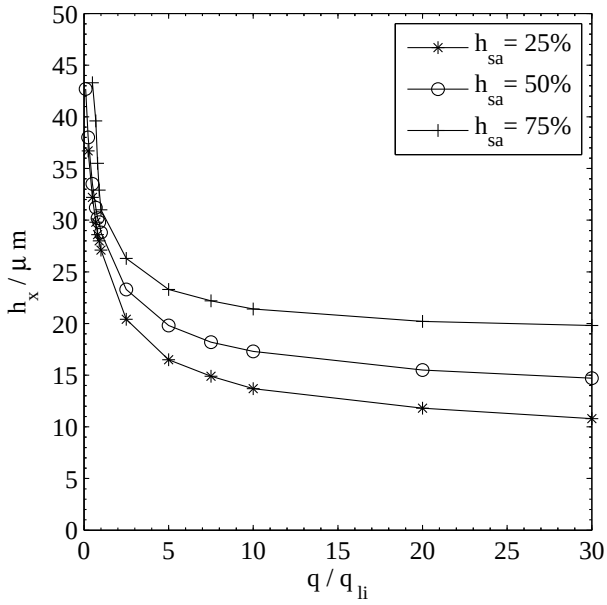

Figure 3.9: The position of the sample flow h_x as a function of the flow ratio q/q_{li} at a flow rate of $q = 1\,\mu$L/min and a lateral length of the inlet x_{inlet} of 100 % of the channel height $H = 50\,\mu$m. The parameter is the entrance height of the sample flow h_{sa} relative to H

liquid and not the channel walls. The concept for the developed devices is as follows. First the sample flow is injected through an inlet in the bottom into the sheath flow, forming a non-coaxial sheath flow. This combination gets horizontally compressed by the taper afterwards. Passing the uplifting port produces a vertical coaxial sheath flow. In the last step the side ports allow further compression of the horizontal width.

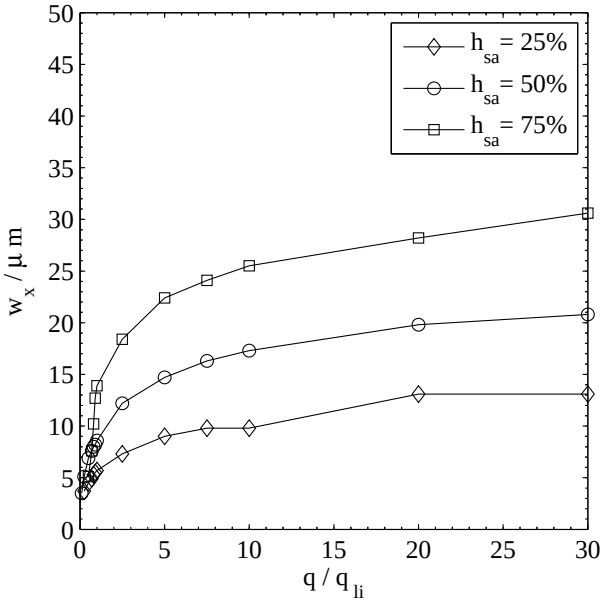

Figure 3.10: The width of the sample flow w_x after passing the uplifting port. Parameters similar to Figure 3.9.

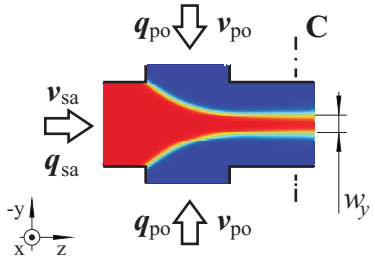

Figure 3.11: The influence of symmetric side ports ($q_{sa} = 1\,\mu\text{L}/min$ and $q_{po}/q_{sa} = 1$)

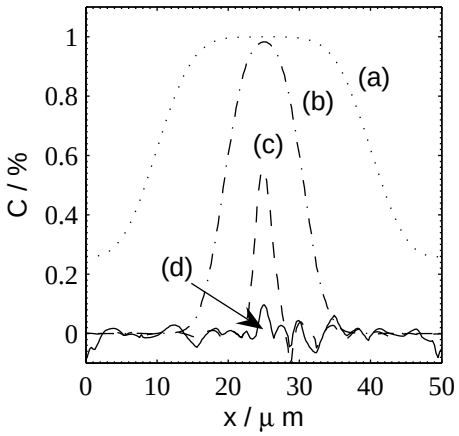

Figure 3.12: Varying concentration at position C and $q_{sa} = 1\,\mu\text{L}/min$: q_{po}/q_{sa} =(a) 0.1, (b) 1, (c) 10 and (d) 100

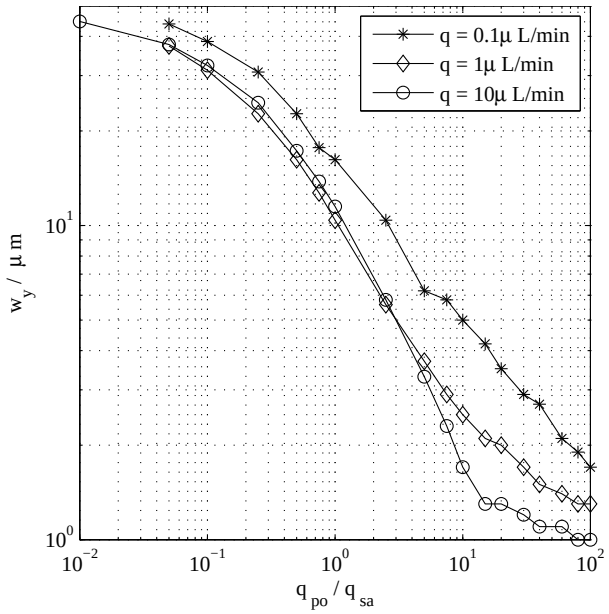

Figure 3.13: The correlation between the achievable width of the sample flow w_y and the flow ratio q_{po}/q_{sa}

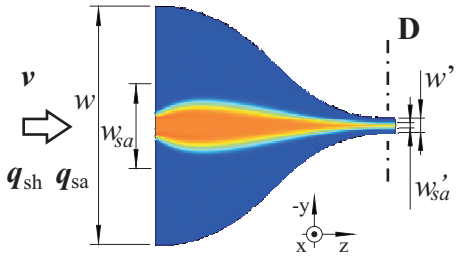

Figure 3.14: Top view of a taper ($q_{sa} = 1\,\mu\mathrm{L}/min$ and $q_{po}/q_{sa} = 1$, $w = 800\mu$m, $w_{sa} = 80\mu$m, channel height 50μm)

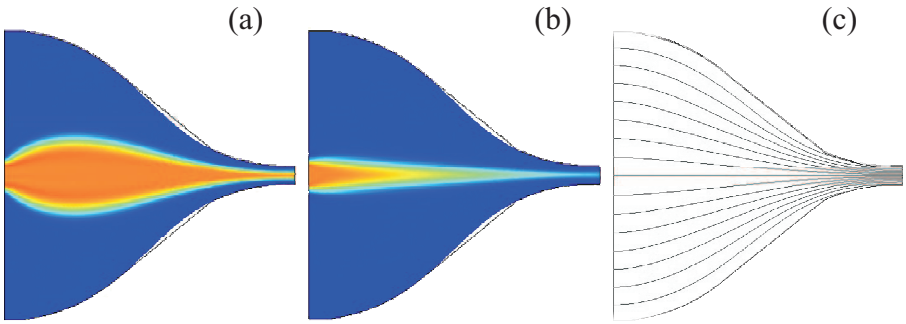

Figure 3.15: Increasing the flow ratio q_{sh}/q_{sa} = (a) 0.5, (b) 5 illustrates how the influence of diffusion gets less. (c) Shows a streamline plot without the influence of diffusion. Sample flow rate $q_{sa} = 1\,\mu\text{L}/min$.

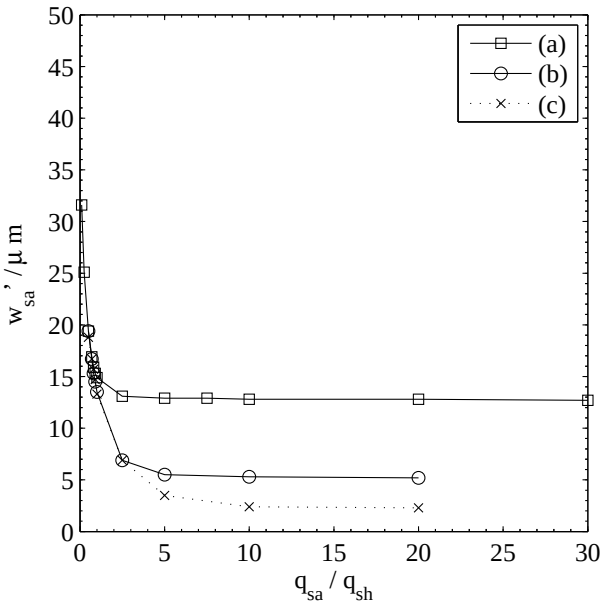

Figure 3.16: The sample width w'_{sa} influenced by varying absolute values of q_{sh} and the diffusion constant D, measured at position D. (a)$q_{sh} = 0.1\,\mu\text{L/min}$, $D = 1 * 10^{-9}\,\text{m}^2/\text{s}$, (b)$q_{sh} = 1\,\mu\text{L/min}$, $D = 1 * 10^{-9}\,\text{m}^2/\text{s}$, (c)$q_{sh} = 10\,\mu\text{L/min}$, $D = 1 * 10^{-10}\,\text{m}^2/\text{s}$

Chapter 4

Design and Fabrication

Based on the preliminary considerations and the results of the theoretical simulations, discussed in the former chapter, the following designs have been developed (see Table 4.1) and two device holder concepts for the experimental setup, as shown in Fig. 4.9 and Fig. 4.10, were realised.

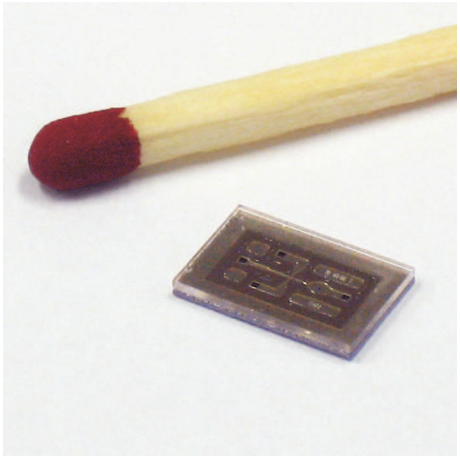

Figure 4.1: Size comparison of device No. 1, $6 * 9\,\text{mm}$ chip size and $900\,\mu\text{m}$ thickness.

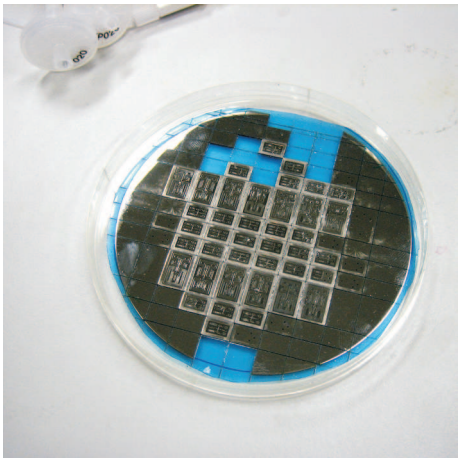

Figure 4.2: The fabricated 100 mm wafer, showing the relative size of the two chip sizes.

Compared to the rather complex conception used in the work of *Narajan Sundarajan* [4] the microdevices presented in this thesis consist of three parts: A silicon body, a glass cover and polymer-based thick resist layer (SU-8) which defines the shape of the channels. The technology of SU-8 based lithography and low temperature wafer bonding is used as discribed in [18]. For taking measurements the microdevice is mounted onto a disposable supporting panel (see 4.2.3). This unit is fixed onto a, so called, holder that represents

the connection to the pipes, which are fed by several syringe-pumps delivering the fluids. The panel and the holder allow comfortable handling of the microdevice during the experiments.

4.1 Design of the Devices

4.1.1 Principal structure of the microdevices

The bottom of the microchannel is made of silicon (360 μm thickness) and the channel top is defined by a 500 μm thick Pyrex glass plate. The connection holes to the outside are KOH-etched into the silicon. The microchannels are made of SU-8, see [18]. The height of the SU-8 layer of 50 μm defines the overall channel height.

4.1.2 General design considerations

To maximize the output and to increase the research possibilities it was considered as an asset to develop several different types of devices and to put them onto the same wafer. The designs differ in their channel geometry, the hydrodynamic principle and in the holder concept they use. The general design criteria were:

- minimum dimensions of the formed sample flow, goal 2μm
- inlet and channel dimensions, as large as possible to avoid clogging effects. The inlet dimensions were chosen to be mainly 50 μm in square.
- chip dimensions as small as possible
- a holder concept, constructed in a simple way and easy to handle

A list of all designs that could be realised is given in 4.1. For the sake of completeness the missing device No. IV is explained by the fact that this design was not considered worth to be fabricated and therefore left out.
The total number of different designs is five and they were arranged in a mixed pattern on the silicon-wafers to eliminate the risk of the total loss of a design due to fabrication mistakes. The position on the wafer of the different devices and their arrangement shows Figure 7.1. To make the arrangement of the different designs easier and, under the aspect of minimum space requirements, more efficient, their surface dimensions had to be identical or in multiples. It was found that chip dimensions of $6 * 9$ mm and $9 * 13$ mm are the best choice from the technological point of view (diameter of the

Design Name		Hydrodynamic Principle		Holder Concept	
#	Wafer Label	COAXIAL	NON-COAXIAL	6 x 9 mm	9 x 13 mm
I	I.COAX	X	-	X	-
II	II.COAX	X	-	-	X
III	III.COAX-S	X	-	X	-
V	V.N-COAX	-	X	-	X
VI	VI.N-COAX	-	X	X	-

Table 4.1: Names and labels of the fabricated designs together with their main characteristics

available hoses, fabrication efforts of the silicone gasket and the mounting and handling of O-rings). These dimensions include some extra space to the edges for the sealings and space for bonding pats for electrical connections, if needed. The plain lateral dimensions of the microfluidic system are just $4 * 7$ mm and $7 * 12$ mm. 60 devices could be placed onto the 100 mm wafers, 46 small and 14 large devices.

Due to the fabrication technique the channel height is the same for all designs on the same wafer. For future batches it could be worth to try to produce chips with a channel height of, for example, the half of the value of the first batch. This would result, for the device No. III in a square cross section of the main channel and would allow further studies of the influence on the shape of the sample flow.

If the designs are distinguished by their hydrodynamical principle then there are two groups: The coaxial and the non-coaxial devices. The first are the coaxial sheath flow devices (three different designs), which also represent the novel and more interesting ones. The second group uses the non-coaxial principles (two designs). The non-coaxial devices represent some kind of "rescue"-designs. They are designed in a simple way with dimensions that are not too critical to fabricate and have no inlets which are too small (clogging can not that easily occur). These designs are not able to deliver such small sample flow dimensions like the others are expected to give. On the other hand these "rescue"-designs will give guaranteed evaluable data, for the case fabrication of the more critical designs fails.

As it is discussed in the next chapter, a novel sealing technique was used for the connection between the microchip and the holder. To get a clear comparison to the conventional sealing technique, with standard O-rings, it was decided to fabricate both. This resulted in two different chip sizes and therefore the realised designs have to be distinguished by their chip size and the type of holder that has to be used in the experimental setup (see next chapter for further details).

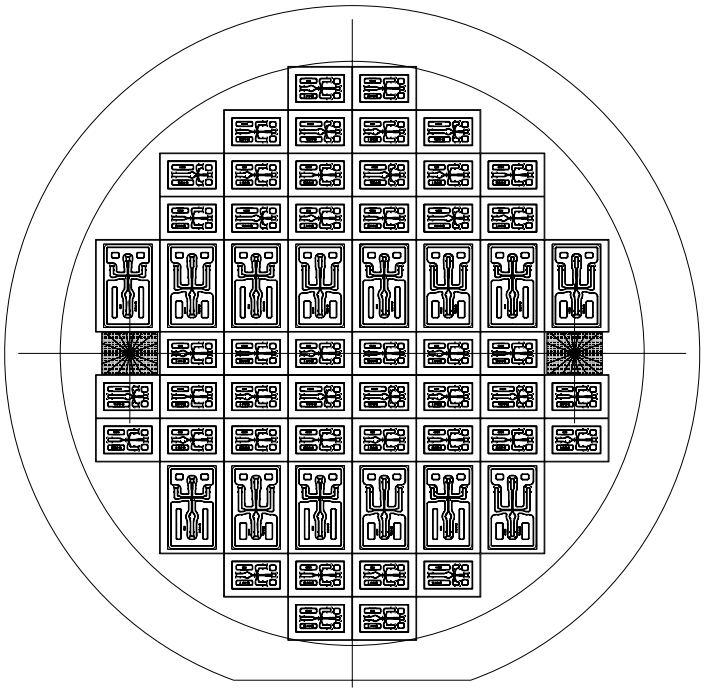

Figure 4.3: ACAD layout of the 100 mm wafer. The layouts of the single lithographic masks can be found in the Appendix 7.1.

The measurement technique for the analysis are optical methods (optical fluorescent microscopy and confocal laser-microscopy). If required, there is always the opportunity for doing impedance measurements (Coulter counter) with the non-coaxial devices, as well. For this, electrodes can be easily integrated by simply including an additional mask for the silicon wafer in the fabrication process.

4.1.3 Chosen Designs and Layouts

The purpose of this part is to give a description of the designs which were fabricated. Together with the desired purpose, the design characteristics are listed. The overall height of the channel structures was 50 μm . This results in an aspect ratio of one and a square cross section of the main channel for all designs, except for the design No. III.

Device No. I

Desired purpose: This device gives a sample-flow diameter in the range of 2 μm and represents the device on which the main focus of interest was held. It can be used as an alignment tool for example to position Escherichia coli bacteria for optical detection and analysis.

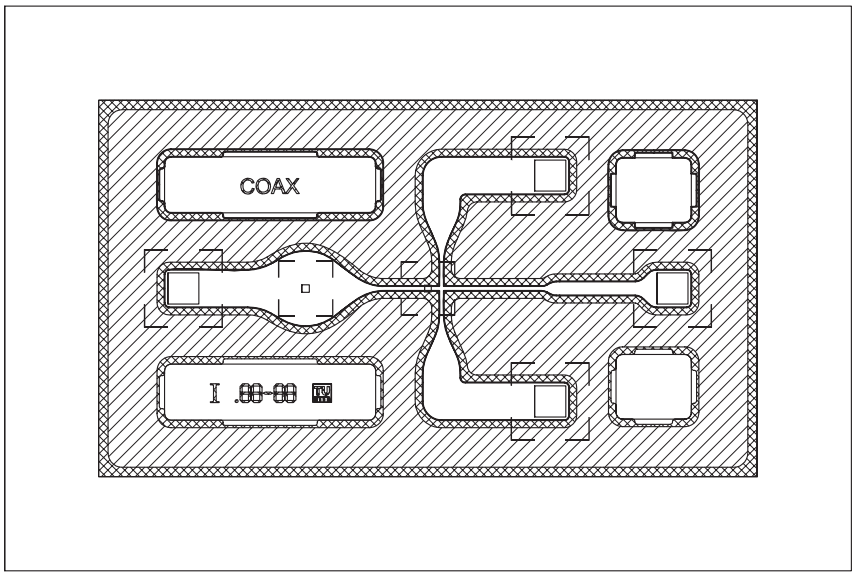

Figure 4.4: Coaxial device No. I, small chip size. The double hatched area indicates the hardened SU-8, the single hatched soft SU-8 for improving the tightness and strength. The dashed lines represent the etched cavities.

Design characteristics: The sheath liquid passes the inlet ($330*330\,\mu m^2$) in the bottom of the channel and is led toward the sample inlet ($80*80\,\mu m^2$). The inlet area has a channel width of 400 μm and expands to 800 μm. The sample is led through an $80*80\,\mu m^2$ inlet. The transversal compression of the taper is from 800 μm to 50 μm which gives a factor of 16. The uplifting inlet in the bottom of the channel is $50*50\,\mu m^2$ large and the two side ports, following from the side, have a cross section of $50*50\,\mu m^2$. For analysis an almost 1 mm long straight section (50 μm width) after the sample forming took place follows before the channel expands again to 160 μm width. This section is also of 1 mm length and gives further space for taking measurements. This broader channel section gives the possibility to measure the

expanded sample flow diameter with less resolution requirements for the optical detection equipment but accepting the drawback of a lowered contrast. Finally the channel expands to 400 μmm channel width and leads to the drain of the device ($330 * 330\,\mu\text{m}^2$). The device is connected via the moulded silicon-packing to the holder.

Device No. II

Desired purpose: From the hydrodynamical principle this device is designed similar to the first and differs only in the chip dimensions. This device to *Holder B*, the holder with the O-ring gasket.

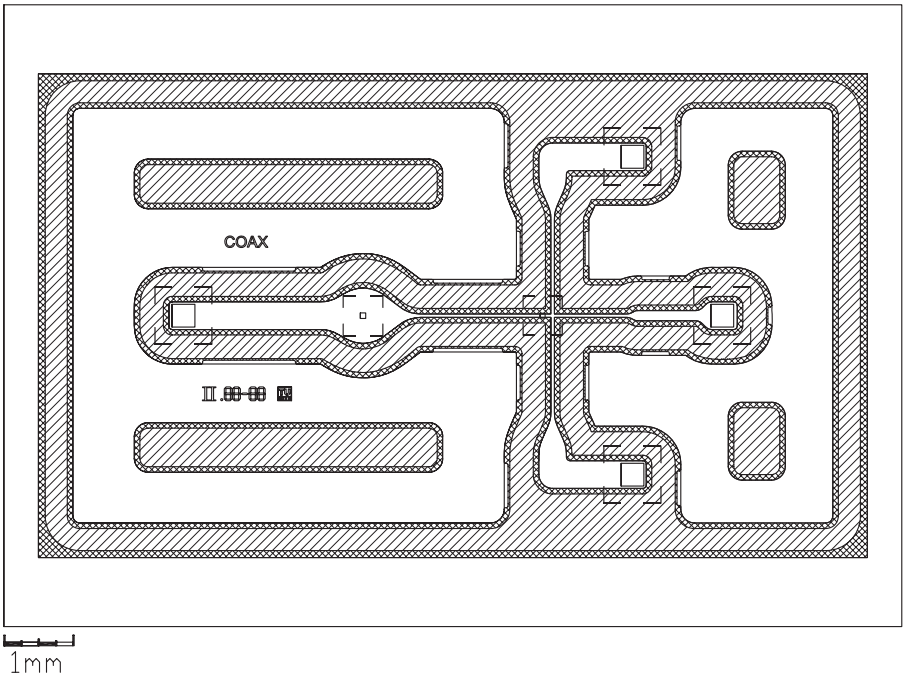

Figure 4.5: Coaxial device No. II, large chip size.

Design characteristics: The fluids pass the same sections as in the first design, mentioned above. Only the distances are extended. As a drawback of this design one could mention that diffusion takes place more significantly in the longer channel sections especially between the sample inlet and the up-lifting port. This results in an increased sample diameter caused by the diffusion process and depends therefore strongly on the diffusion constant of the sample liquid.

Device No. III

Desired purpose: The purpose is to minimize the sample flow diameter to technological and detectable limits. A channel width of only 25 μm was considered from the technological point of view as the minimum (aspect ratio of 2 : 1).

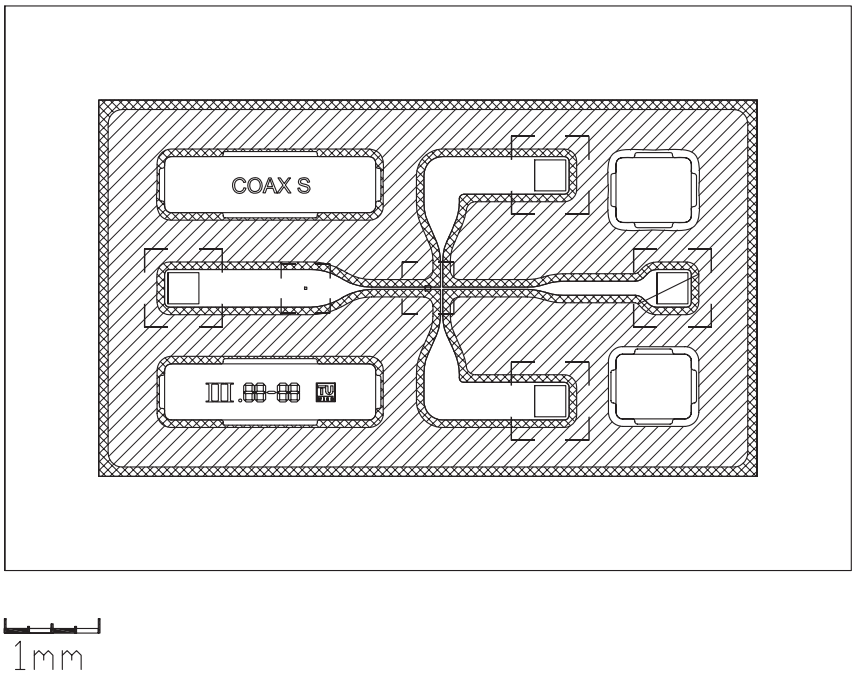

Figure 4.6: Coaxial device No. III, small chip size. 25 μm width of the main channel.

Design characteristics: The design will offer the opportunity to achieve even smaller sample flow dimensions than with the other designs due to the smaller channel geometries. It gives also the opportunity to experiment with the fabrication parameters and to optimize them. Design characteristics: The hydrodynamic principle is like the one of devices No. I, illustrated above. The channel width is about 25 μm. The factor of the taper is 16 (from 400 μm to 25 μm) and the sample inlet is about 25 μm in square. The fabrication tolerances are the limiting factors for the smallness of the inlet holes in the bottom of the microdevice.

Device No. V

Desired purpose: This design should bring measurable results in any case with even smaller sample flow dimension limits than those which were achieved in previous studies. To be prepared for the worst case that the novel sealing of the new holder concept fails, too, it uses the holder with the conventional O-rings (*HolderB*).

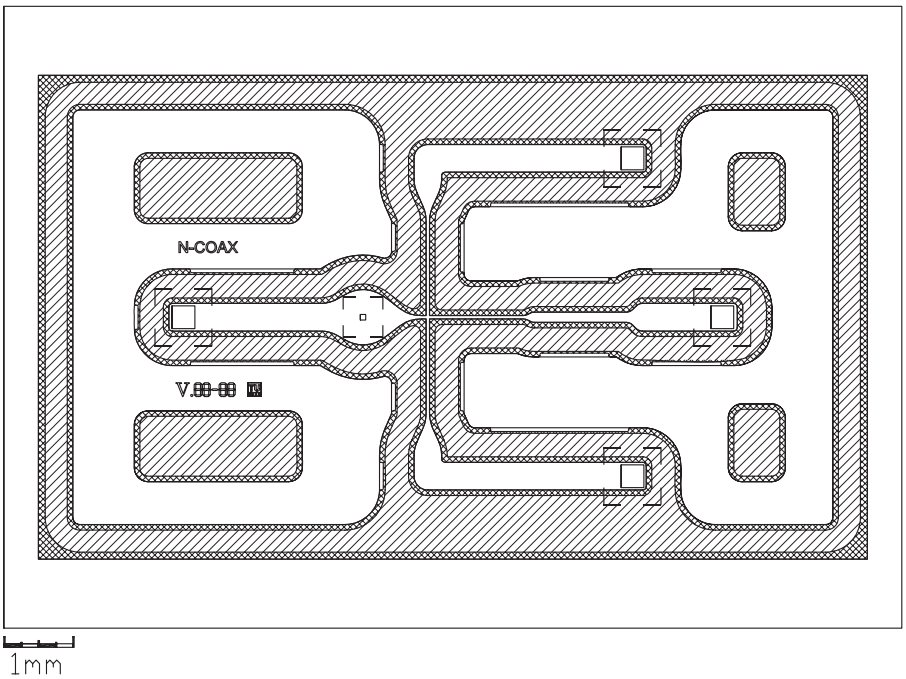

Figure 4.7: Non-coaxial device No. V, large chip size.

Design characteristics: Simple non-coaxial design, similar to the one used in [14]. It gives the opportunity to integrate electrodes easily by adding a lithographic mask to the fabrication process.with integrated Coulter counter. The device is supported by the device holder with O-rings. After the side ports three channel sections, each 1 mm long, are available for taking measurements (50, 160 and 400 μm wide).

Device No. VI

Design characteristics: Non-coaxial design, similar to the device No. V but supported by the device holder with the silicone gasket.

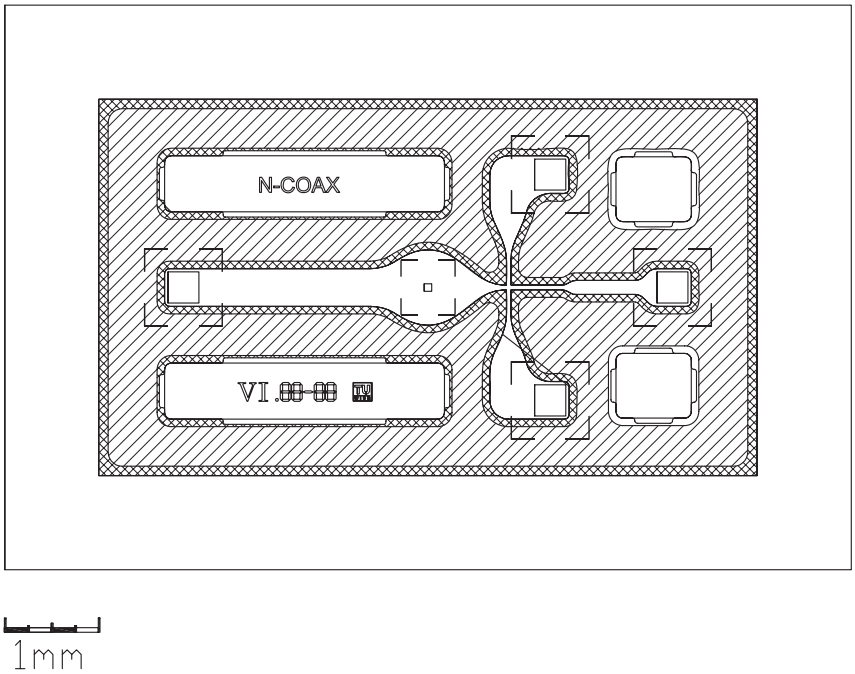

Figure 4.8: Non-coaxial device No. VI, small chip size.

4.2 Design And Conception of the Auxiliary Parts

4.2.1 The holder concepts

The purpose of the so called holder is to provide a tight, rigid and stable connection between the microdevice, the pipes and the rest of the periphery. To avoid any leakage, a gasket is in between. As illustrated in previous works, e.g. of [1], O-rings are the standard way to achieve a proper connection. These gaskets need to be snaped into a notch to keep them in the right position. As it is the aim of this work to scale down the chip size as far as possible, it was necessary to think about the limits of this type of sealing and possible alternatives.
The starting point for the design process of the holder was evaluating the minimal radial separation of the inlets. The criterion was to keep them as close as possible to avoid diffusion between the different focusing stages. It was found that, in general, the limiting factors for holders of such microdevices are first, the outer tube diameter and second, the thickness of the used silicon wafer. The fact that only Si wafers of certain thickness where available made the second argument the dominant one. That is because, as described in

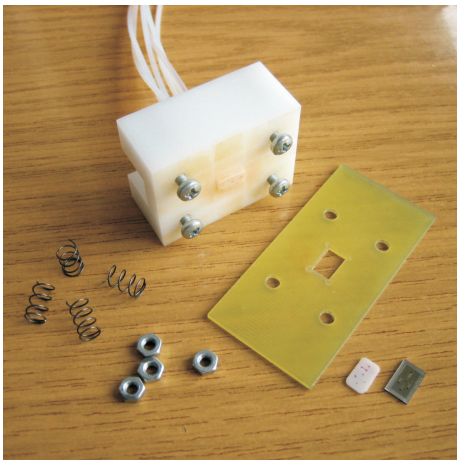

Figure 4.9: *Holder A* together with all required parts

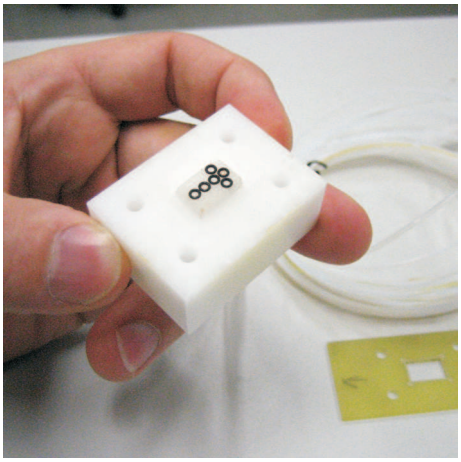

Figure 4.10: *Holder B showing the arranged O-ring seals*

Chapter 4.3, the fluidic holes through the Si-body are etched into the monocrystalline material, generating a pyramid-shaped hole. These etched holes have sidewalls with a fixed inclination (35.26°) to the perpendicular of the surface. The used silicon wafers had a thickness of 360 μm. Considering the fabrication tolerances, the required clearance for the inlets (at least 100 μm). and twice the thickness of the used tube (typically wall thickness 0.2 mm) defines a minimum radial separation of 1 mm. That means that tubes with an outside diameter of 1mm are the limit if Si-wafers of such a thickness are used. For the devices presented in this work, based on these considerations and the available material in the lab, a tube diameter of 1.6 mm (inside diameter of 0.5 mm) was chosen and so the main design parameter for the holder defined.

As in the introduction illustrated, two different holder concepts with different sealing techniques were realised. The conventional design uses O-ring gaskets (outer diameter of 2.6 mm and an inside diameter of 1.4mm). The connecting holes are arranged in the minimum distance from each other that is possible (2.6 mm), see Fig. 4.10.

The second type of holder, *Holder A* uses a cast silicone gasket. It covers and therefore seals the whole area between the holder and the microdevice instead of only small annular areas, as it is the case with O-rings. This sealing technique allows also realisation of straight or curved connecting channels. This allowed reducing the distance between the inlet holes further. As it can be seen in the drawing, Figure 4.11, the sample port could be shifted out of the axis of symmetry. A detailed cross section is given in Fig. 5.6. The connection between the tube of the sample fluid and the inlet into the

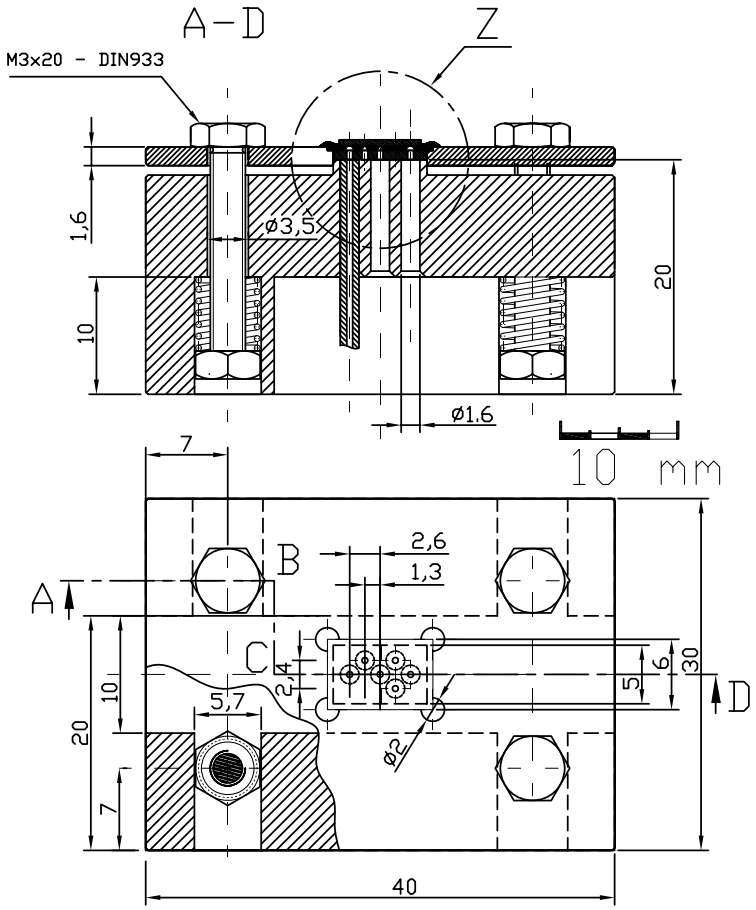

Figure 4.11: ACAD drawing of *Holder A*. See also the detailed cross section (indicated by Detail Z) and the object description in Fig. 5.6.

microdevice is defined by the straight slit in the silicone gasket (see drawing in Figure 7.5).

4.2.2 Silicone Gasket

The gasket was fabricated with a custom build mould. Metal pins and milled structures define the shape of the silicone gasket. Figure reffig:mould shows the technical drawing of the mould and the Picture reffig:BILD-silicone shows injecting the liquid silicone into the closed mould. Liquid silicone rubber from *Wacker Chemie AG* was used. The liquid silicone is mixed to homogeneity in a ratio of 9 : 1 with a curing liquid. The mould is closed and the mixed composite is pumped into the injection hole with a conventional syringe. The mould has to be kept in vertical position to allow air bubbles finding the way to the outlet. This type of silicone rubber cures at room temperature. This takes several days but can be accelerated to less than a hour by heating up to 60°C.

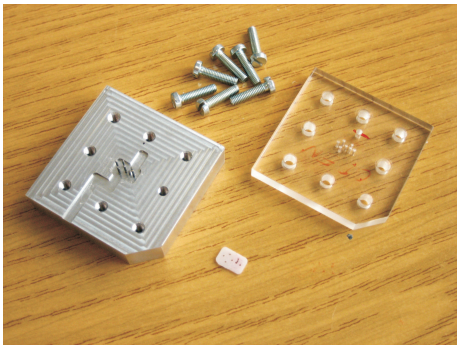

Figure 4.12: Top view of the dissembled mould. The PMMA cover, the milled Al-body and metal pins define the geometry of the Silicone gasket. A moulded gasket lies in front of the other parts. See also Fig. 7.5.

Figure 4.13: Injecting the liquid silicone mixture by means of a conventional medical-syringe into the mould. The mould is kept in an upright position for curing to allow air bubbles leaving the mould through the drain.

4.2.3 PCB-Panel

Due to the small dimensions of the silicon microdevices and their sensitivity against mechanical stress it is necessary to mount the device on a disposable

supporting panel. Additional onboard electronic equipment and connections between the chip and its peripheral parts can be mounted onto this panel if required. It is made from a printed circuit board (PCB for short). Figure 4.15 shows the fabricated panels for the holders. The microdevice gets mounted onto the PCB-panel with cyanoacryl glue and connected via a screw-spring-nut combination with the holder body (see Chapter 5.1 for the detailed setup procedure).

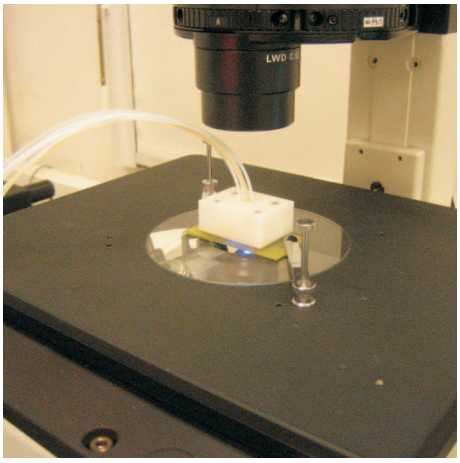

Figure 4.14: The table of the microscope together with the mounted holder, panel and the connecting pipes.

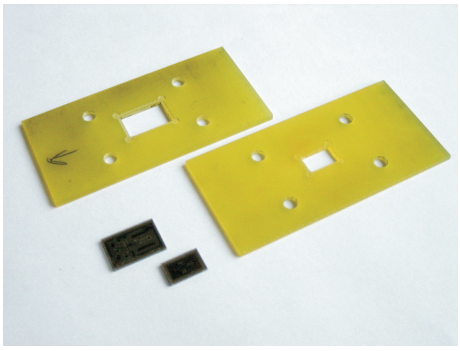

Figure 4.15: The micro devices and the milled disposable panels, made from conventional epoxy-resin glass fiber.

Figure 4.14 illustrates how the panel allows the holder to be fixed onto the table of the microscope with conventional slide-brackets. The detailed cross section of the assembled setup is given in Figure 5.6.

4.3 Microdevice-Fabrication Issues

The details about the fabrication process of the microdevice itself are presented in this section. The fabrication technique of using thick resist lithography is described in the book *Fundamentals and Applications of Microfuidics* [7]. Prior to this work several investigations were done using the SU-8 and low temperature bonding technique by *Peter Svasek* like for example in [18]. The fabrication of MEMS-devices is technologically and historically based on the semiconductor microchip production. Therefore the fabrication techniques for coating, structuring and handling are under excellent control. The whole fabrication and clean-room logistics were carried out on 100 mm wafers. Silicon wafers of 360 μm thickness, with a standard {100} lattice orientation,

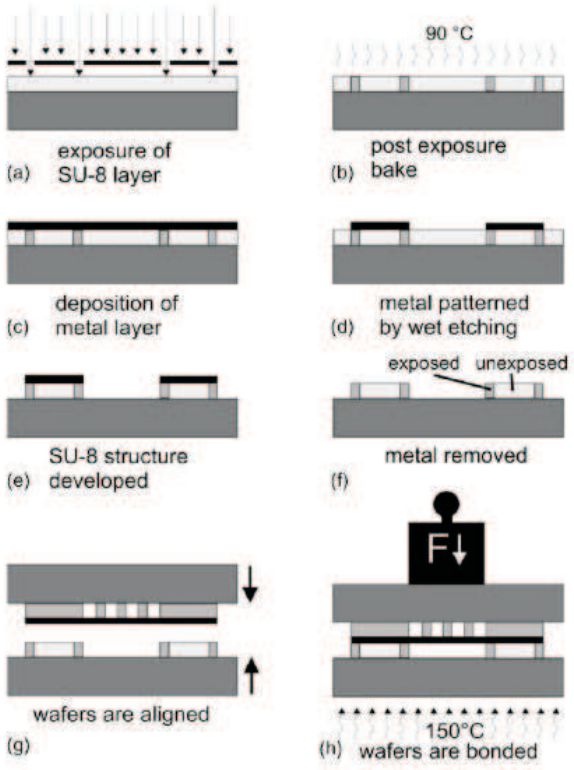

Figure 4.16: Fabrication steps of the improved SU-8 wafer bonding technique. Taken from [18].

n-doped and with nitrite coatings on both sides were used. To allow optical analysis the covering plate of the device has to be at least transparent for the wavelengths of the exciting and the emitted fluorescent light. PYREX-glass was chosen of 500 μm thickness. The channel structure was defined by a lithographically processed epoxy resist SU-8 (negative-working). High aspect ratios, chemical inert channel walls make the use of such polymer based techniques a good choice for microfluidic devices (compared with wet-etched glass structures like in [19] far better optical edges are achieved). It is a negative photoresist based on EPON SU-8 epoxy resin. It shows low absorption in near-UV and allows therefore with photo lithography high aspect ratios. The standard SU-8 photoresist consists of three basic components. EPON SU-8 epoxy resin, a solvent (gamma-Butyrolactone) and a photoinitiator (e.g. triarylium-sulfonium salts). The achievable thickness is mainly defined by the viscosity of the SU-8 photoresist. The choice of using a thick film resist instead of cast silicon elastomer like in [20] was mainly due to the

experience of the department in that field. Of course physical facts like for example the better biocompatibility is also working to ones favour by using the SU-8 technique. The process flow of the microdevice fabrication was as follows and illustrated in Figure 4.16.

1. The Si wafer gets coated with a titanium layer to improve the bonding between the Si wafer and the SU-8 afterwards.
2. An anisotropic wet etching technique (KOH as an alkali hydroxide etchant) is used to process the connecting holes.
3. The glass wafer is spin coated with SU-8 50, soft baked at 95 °C, on a hot plate with flat surface, and exposed through a lithographic mask by near-UV (a).
4. The exposed area gets selectively cross-linked by a following post exposure bake (b) at 90 °C (avoids stress and damage of the film). Afterwards the polymer photoresist is developed.
5. A sacrificial silver layer is applied (c) and patterned by an wet etching process (d) to cover selectively unexposed parts of the SU-8 photoresist of the next step.
6. The SU-8 gets hard baked to give the resist its final mechanical strength and chemical stability.
7. The unexposed and unprotected photoresist gets removed (e). Only the polymerized SU-8 and the covered SU-8 remains.
8. The sacrificial layer gets removed (f).
9. The Si and the *PYREX* wafer are aligned (g) and connected by an adhesive bonding process (h) at 150 °C as described in [18].
10. The bonded wafer gets cut.

Chapter 5

Experiment and Measurements

5.1 The Experimental Setup

The setup can be divided mainly into four groups. It consists of the microdevice itself, the fluid-pumps (Fig. 5.2 and syringes, a unit that connects them (panel, holder, pipes and filter, see Fig. 5.3) and an analytical unit (optical microscope, Fig. 5.1). The used microscope, *Nikon Digital Eclipse C1*, allows conventional and confocal fluorescent laser microscopy. The setup with holder *A* is shown in Figure 5.1.

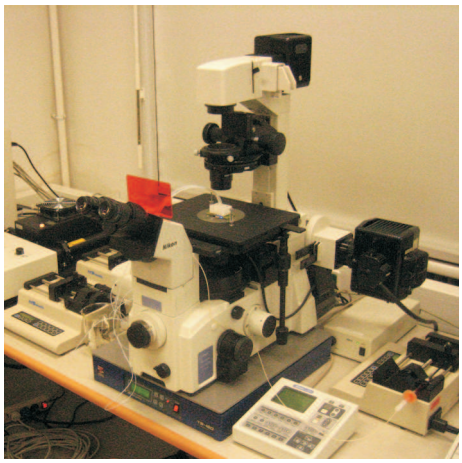

Figure 5.1: The confocal laser microscope *Nikon Digital Eclipse C1*.

Figure 4.14 and Figure 5.5 illustrate that it is necessary to mount the microchip headlong onto the table of the microscope. The connection between the holder body and the syringe pumps was achieved via conventional polymer-silicone pipes (inner diameter 0.5 mm, outer diameter 1.6 mm) with

1.2 m length. The syringe pumps are stepping motor driven and the parameters can be programmed freely. One pump allows driving two syringes at once. Three pumps (*KDScientific Model 200*) were available from the lab. Two of them during experimental use shows Figure 5.2.

Figure 5.2: The *KDScientific Model 200* syringe pumps allow to drive two syringes at once.

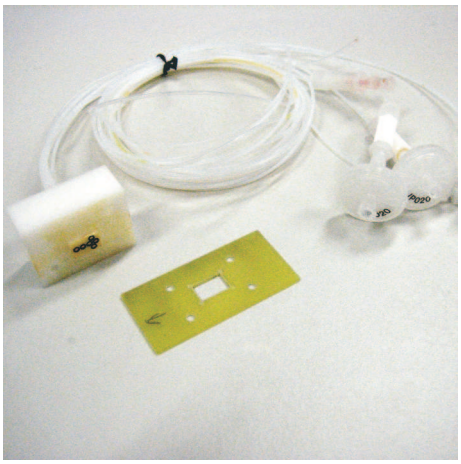

Figure 5.3: Holder B together with the auxiliary parts (panel, pipes and fluid filter units.

Due to the fact that the coaxial microdevices require five different sources of fluids it was necessary to combine some of them and to drive them with one pump. For the side ports this is easily accomplished if a symmetric sheath flow is desired by using two syringes of the same size. During the experiments and depending on the measured parameters various combinations of the sample, sheath and the uplifting ports were used. Using different sizes of syringes (1, 2.5, 5, 10, 25 ml) allows to get various fixed flow ratios between two sources. The necessity to combine different fluid sources limited the choice strongly of varying them independently of each other.

The setup procedure

The microfluidic chip gets mounted onto the panel via conventional cyanoacryl glue. Using such a inviscid glue brings a fast and rigid connection and the side effect that the glue creeps inside the split of the glass cover and the silicon part providing an essential improvement of the SU-8 bond. This strengthens the bond and results in longer durability of the used microchip, see the technical drawing Fig. 5.6. The syringes are filled with de-ionized water and diluted Acridin-Orange. To avoid air-bubbles inside the pipes these liquids are driven through the pipes and the holder before the panel and

the microchip is mounted onto the holder. After rinsing the auxiliary parts the microchip is fixed onto the holder. Bolts that are supported by springs ensure a soft contact pressure for the brittle Silicon microchip. In the last step the panel is strapped onto the table of the microscope with conventional slide-brackets.

5.2 Measurement Methods

Confocal laser scanning microscopy is a microscopic technique that allows to obtain high resolution images and 3-D reconstructions of thick specimens at various depths. The computer controlled microscope focuses onto a specific focal plane and scans and detects the fluorescent area of interest point-by-point. Doing this for several neighbouring focal planes allows reconstruction of the vertical information and generating volume-render models of the collected data. The picture in Figure 5.4 illustrates the principle of confocal microscopy. The confocal laser microscopy in use shows Fig. 5.5. A more detailed insight into the confocal laser scanning microscopy can be found at the online-dictionary *Wikipedia* [21].

5.3 Measurement Results

The detailed measurements presented in this chapter were done with the coaxial and non-coaxial microdevices No. 1, No. 2 and No. 6. on holder *A* (see Table 4.1).

5.3.1 The Sample Inlet

The confocal measurements reveal 3D insights into how the sample flow enters through the bottom of the microchannel. The longitudinal flow profile shows the same lateral shape and size as in the theoretical models (see 3.1.1). At higher flow ratios q_{sh}/q_{sa} it seems that no stable flows can be achieved and that no further sample flow is emitted. Explanations for this could be the back flowing sheath liquid (see Fig. 3.5) or either missing balance of the flows, caused by flushing processes as described below.
The etched holes in monocrystalline substrates bear a pyramid-shaped cavity with a huge volume of several cubic millimetres below the surface, see the technical drawing in Fig. 5.6. To remove air bubbles and small particles like dust it is necessary to flush the device from time to time during the experiment. This causes the cavity below the sample inlet to be filled completely with sheath liquid. Continuing an experiment after this and considering high

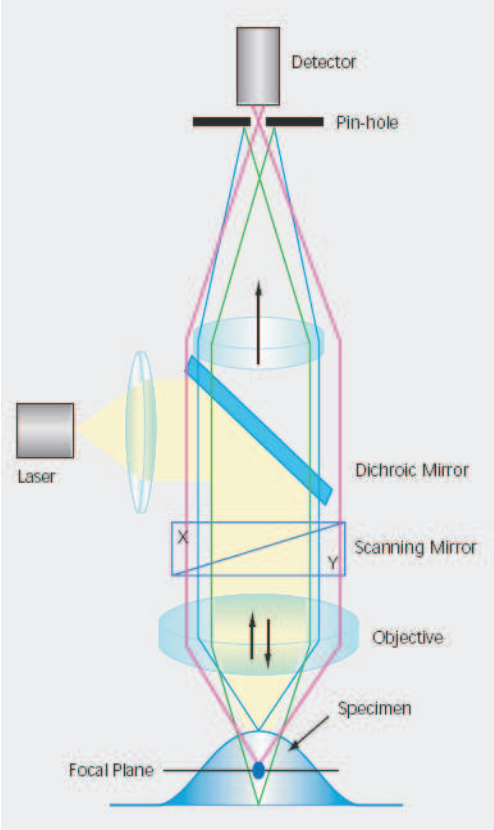

Figure 5.4: The principle of confocal laser scanning microscopy. The pin-hole ensures that only beams from a certain focal plane reach the detector.

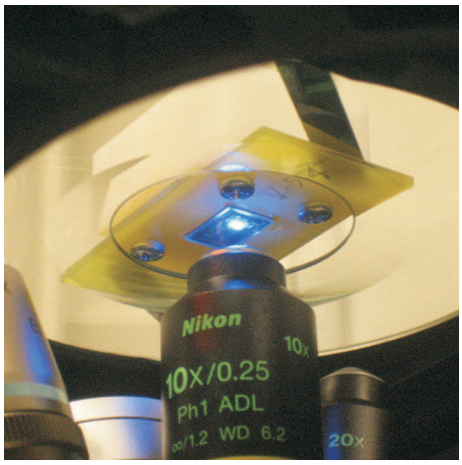

Figure 5.5: The microfluidic chip mounted headlong onto the table of the microscope. Seen from below, showing the objective lens and the scanning laser light reflected by the microchip.

flow ratios of q_{sh}/q_{sa} at low absolute values, like $q_{sa} = 0.01\,\mu$L/min results in the effect that no sample liquid seems to be emitted at those values. In reality sample liquid is emitted, but before entering the microchannel it has to pass the tube and the cavity and to fill these volumes again with sample liquid. At the part with the largest cross section of the cavity the sample velocity is much slower than in the area where the flow enters the microchannel. The factor between the flow velocities is in the range of 50. Strong diffusion takes place between the sample liquid and the sheath liquid in the cavity.

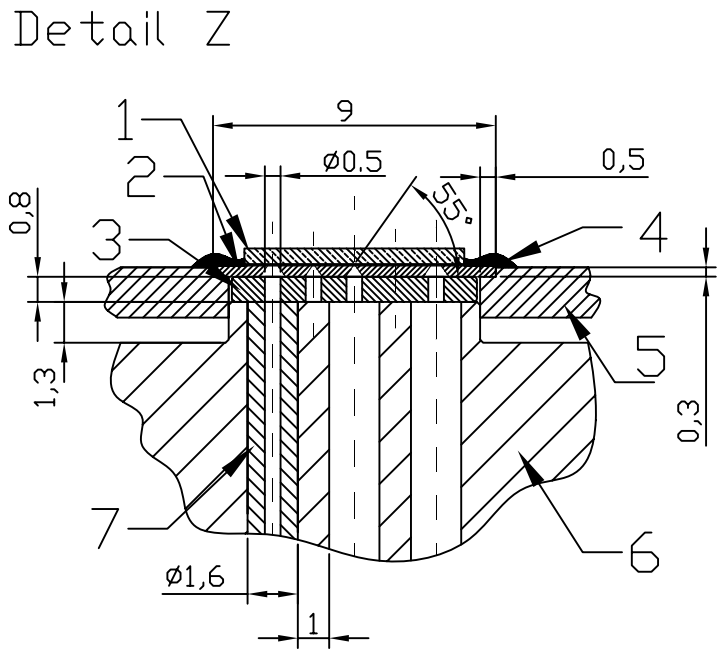

Figure 5.6: Cross section drawing of holder A showing the etched cavities. (1) cover glass, (2) Silicon, (3) silicone gasket, (4) cyanoacryl glue, (6) PMMA holder body and a (7) silicone pipe (shown with only one silicone pipe mounted) . For further description see Fig. 4.11.

This results in long dead-times before stable flow comes back. In the experimental situation it requires relatively long time to get well balanced flows. Figure 5.7 shows a 3D perspective view of the sample inlet. The sample flow enters from the rectangular inlet ($80{*}80\,\mu$m^2) the microchannel and is formed by the sheath flow, flowing from right to the left side. The sample flow inlet in the horizontal plane (y-z) show the pictures in Figure 5.8.

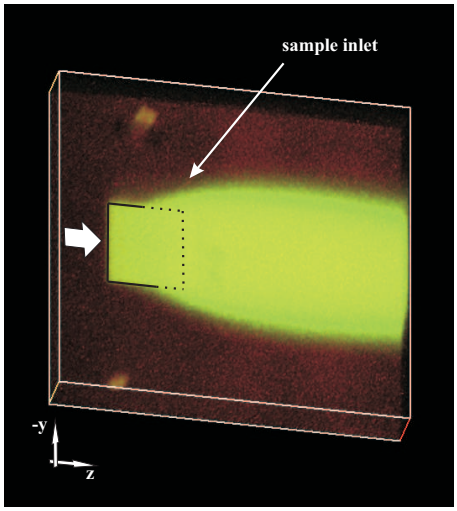

Figure 5.7: Perspective view of the sample flow streaming through the sample inlet into the microchannel ($q_{sh}/q_{sa} = 40$, $q_{sa} = 0.1\,\mu$L/min). The box marks the image area of the confocal measurement.

5.3.2 The Taper

Measurements of the taper compression illustrates the sequence in Figure 5.8. The sequence shows the influence of diffusion and how the shape of the sample width w_y is effected by the flow ratio q_{sh}/q_{sa} above the found limit $q_{po}/q_{sa} = 80$ (scaled by the factor of 16, according to the different channel geometry), described in Section 3.1.4. Direct comparison with the streamline plot in Figure 3.15 (c) shows that the flow ratio is already high enough to assume the smallest sample width w'_y after passing the taper. Increasing the ratio even further has almost no effect on w'_y, only the contrast gets lower together with reducing w_x.

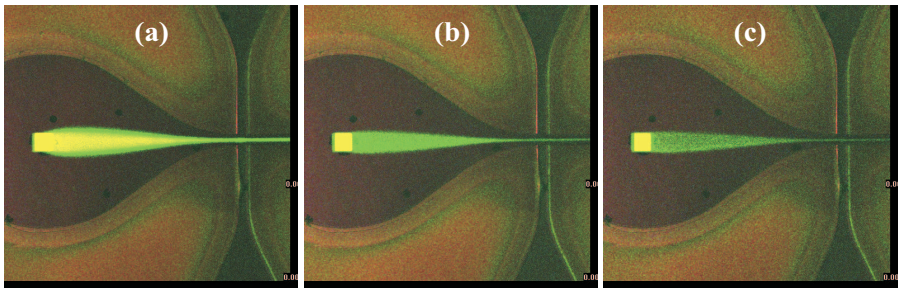

Figure 5.8: Influence of increasing q_{sh}/q_{sa} above the limit of $q_{po}/q_{sa} = 80$ ($q_{po}/q_{sa} =$ (a) 200, (b) 400 and (c) 800)

5.3.3 The Uplifting Port

The use of an uplifting port which raises the non-coaxial sample flow to a coaxial one made it necessary to have analytical equipment that can give additional information about the fluids in the vertical axis. Figure 5.9 shows a lateral cross section oof the uplifting port together with the side ports. Together with Figure 5.10 and 5.11 they illustrate the process of sample forming in the coaxial microdevice No. 1.

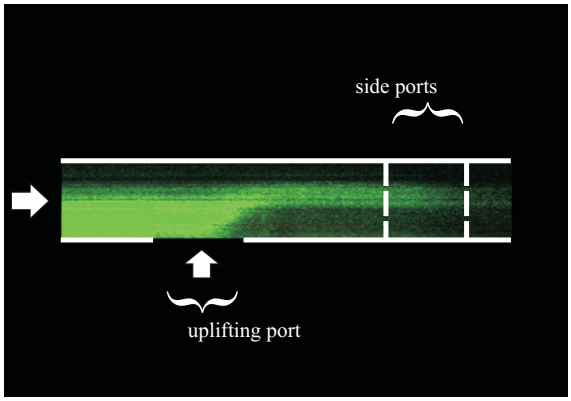

Figure 5.9: Lateral cross section: The influence of the uplifting port on a non-coaxial flow ($q_{sh}/q_{sa} = 25$, $q_{sa} = 1\,\mu$L/min and $q_{li} = 12.5\,\mu$L/min).

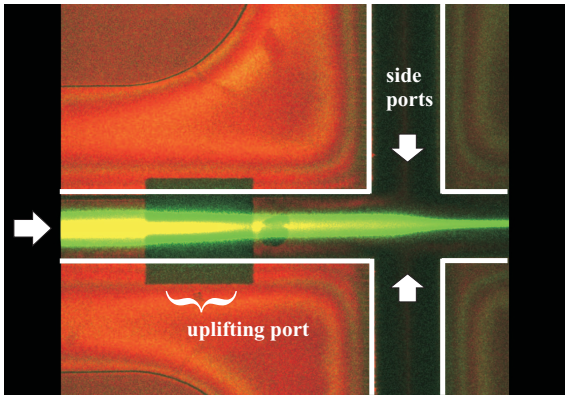

Figure 5.10: Top view (see also Figure 5.9).

Due to the fact that high resolution confocal images with good contrast consist of 100 - 1000 single frames, stable hydro dynamical flows for up to one hour were necessary. Stochastic interruptions caused the noticeable dark lines in the images. The use of the 500 μm thick covering glass made it

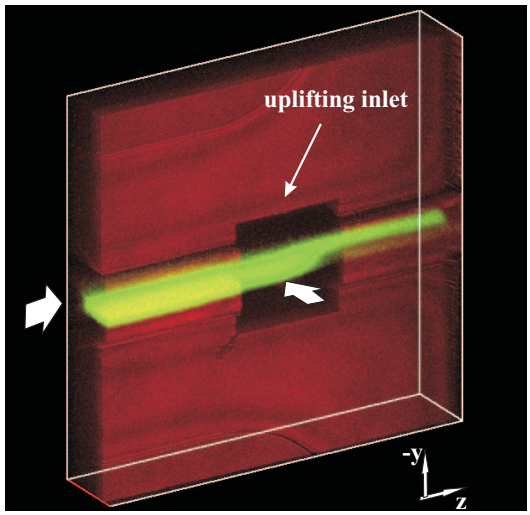

Figure 5.11: Perspective view (see also Figure 5.9).

impossible to use high power objective-lenses. A magnifying power of $x\,40$ was the maximum that could be used and therefore the confocal resolution in the vertical dimension was always a bit low. In addition to this shadowing and mirror effects made it always difficult to catch to right focal planes and to interpret the data correctly, especially at the areas below the sample flow and close to the walls of the channel. The analysis of the sheath flow profiles after each step of sample forming are shown in Figure 5.12.

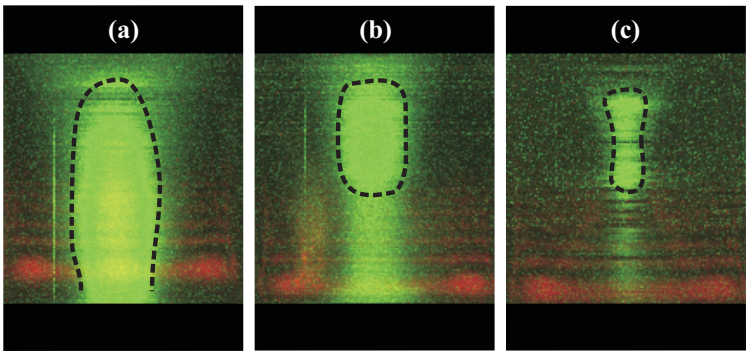

Figure 5.12: Sample flow profiles: (a) before and (b) after the uplifting port. (c) shows the compression of the symmetrically flow of the side ports ($q_{sh}/q_{sa} = XXX$, $q_{sa} = XXX\,\mu$L/min). The dotted line marks the border where in the digital data the contrast drops down to 50%.

5.3.4 The Side Ports

The measurements of the focusing limits that are achievable with the side ports were done in two steps. First, the input flow of the channel was 100% sample liquid without any sheath flow. Second the input flow was a non-coaxial sample flow. Figure 5.13 shows the influence of the side ports with

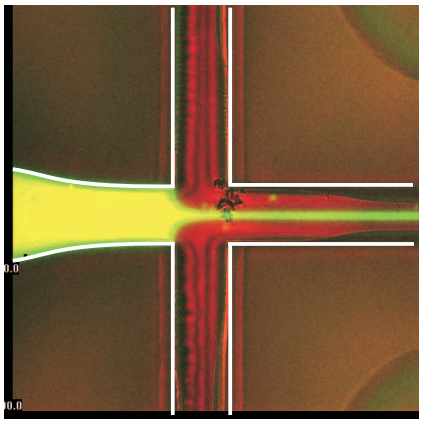

Figure 5.13: Side port pressure forming a double layered sheath flow ($q_{po}/q_{sa} = 10$, $q_{sa} = 0.4\,\mu$L/min). Compression to a width of $w_y = 10\,\mu$m.

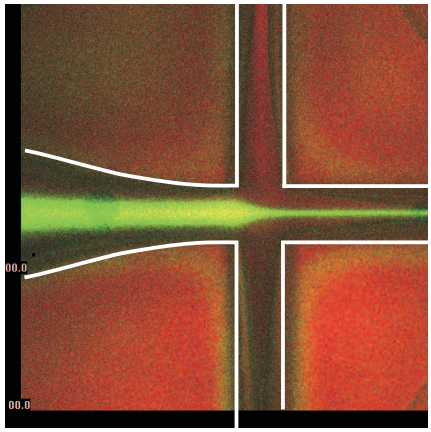

Figure 5.14: A non-coaxial sample flow compressed by the side ports, sample width $w_y = 2.5\,\mu$m ($q_{po}/q_{sh} = 4$, $q_{sh} = 2\,\mu$L/min, $q_{sa} = 0.1\,\mu$L/min).

flow rates of $q_{sa} = 0.4\,\mu$L/min and $q_{po}/q_{sa} = 10$ which resulted in a sample width of around $10\,\mu$m. The use of a non-coaxial sample flow prior to the side ports results in a sample width of $3\,\mu$m ($q_{sa} = 0.1\,\mu$L/min, $q_{sh} = 2\,\mu$L/min and $q_{po}/q_{sa} = 80$), see Figure 5.14. The ratio of q_{sh}/q_{sa} and the taper form a non-coaxial sample flow which has a width of around $17\,\mu$m. Therfore using a taper helps to reduce the sample width by the factor of 2.5.

Chapter 6

Conclusions

To summarize the output of this work and to conclude this thesis, a short discussion and an outlook is given.

6.1 Discussion

6.1.1 Accomplishments

The primary idea of this work was to develop new microfluidic devices, based on the ideas and devices from J. H. Nieuwenhuis, [1], with the aim to analyse the size limitations for the sample flow and the chip size as well. This work shows that five different devices could be developed, fabricated and tested. Prior knowledge could be proved and extended. In addition to this the following things were done:

- To increase the experimental possibilities non-coaxial and coaxial devices were designed and analysed. The decision to add coaxial fluidic devices opened up the opportunities to analyse idle streaming sample flows too. The developed non-coaxial devices could be used to make detailed analysis of the flow profile and uniformity of the sample flow by Gabriel Hairer in [5] and will allow (with an additional mask) impedance spectroscopy like it is described in the work of *S. Gawad* [11].

- The realised coaxial devices are able to focus and align sample streams to the size of several micrometers. In addition to this the devices were realised under the design criteria of minimum sample dimensions achieved with maximum channel dimensions.

- The focusing limits of the coaxial device No. I is about 2.5 $\pm$ 1 μm in the horizontal and 10 $\pm$ 2 μm in the vertical dimension. Preliminary experimental results with the coaxial device No. III showed that this device will be capable to push these limits easily. As the investigations by Gabriel Hairer show, limits of 1.5 $\pm$ 1 μm in the horizontal and 12 $\pm$ 2 μm vertical were achieved.

- The theoretical study and the experimental verification of these coaxial devices gave the know-how to characterize the sample flow by the related parameters. The collected data showed how the size and shape of the channel inlet have influence on the sample and at which ratios the used focusing techniques show the best performance to get the best results.

- The need to analyse even the flow profile of the sample streams made it necessary to find an alternative to conventional fluorescent photography. The most promising technique was the confocal laser scanning microscopy. To our knowledge, detailed confocal laser microscopic measurements and work methodology for microfluidic streams could be achieved for the first time at the department of this University.

- The different designs were chosen under the aspect to give a lot of further applications to future analysis and experiments, such as for flow cytometers and coulter counters, see Chapter 6.2 . Therefore the developed devices still offer a lot of research potential which could be partly used in recent investigations like in [5] .

- Two different holder concepts were realised. One of them, *Holder A* uses a new way of sealing with a moulded silicone gasket. The direct comparison of the two holder concepts showed some significant practical advantages in fabrication and its use.

- The total chip size could be reduced from 14 x 20 mm to only 6 x 9 mm which resulted in higher number of devices per wafer (4 inch size) and therefore in reduced costs per fabricated device.

6.1.2 Unexpected facts

- It seems that sample streams below 5% of the channel width are not possible to achieve. There are at least two different reasons for that: First due to fast sample flow diffusion and second due to high flow rates which are related to focusing to small dimensions. Flow instabilities and oscillations from the syringe pumps, the pipes and unavoidable

micro bubbles inside the channels and especially in the zones of the connections make it difficult to achieve the theoretical limits that have been obtained by the finite element simulations.

- The image quality of the microscope is at least negatively influenced by the covering glass-plate of the microdevice which has a thickness of 500 μm. This weakens the contrast in general and the ability to achieve high resolution in the depth. For the investigations by *Gabriel Hairer* the new batch of wafers were fabricated with covering glass-plates of 200 μm thickness. As it can be seen in the illustrations of the work and the results a much better contrast and resolution could be achieved.

- The holder concept, *Holder B*, with the conventional O-ring seals could not compete with *Holder A* at those small dimensions of the devices: The small O-ring seals showed very little elasticity and therefore only little chances to compensate small gaps. The attempt to avoid larger gaps would result in unreasonably small fabrication tolerances for a proper sealing. In practical use it was sometimes quite difficult to get sealed connections with this holder. The major drawback was the fact that the device was fixed via the PCB-panel onto the table of the microscope. The bunch of six pipes generates always a torque that forces the holder to tilt. Even if the O-ring seals are still tight this results in e.g. unpredictable unsymmetrical flow pressures from the side ports. Of course there are possibilities to support the pipes properly or to fix the microchip via the holder body instead via the PCB-panel, but there are still the high requirements on the tolerances and the problems of O-rings that jump out of their notches during setup. After all, the only advantage of the higher surface pressure can not compete with the comfort of simplicity and effectiveness of the holder concept with the silicone gasket especially if smaller chip dimensions are desired.

6.1.3 Improvable aspects

- In this work the total number of three pumps made it necessary to drive e.g. two syringes with one pump. In such a case only one flow parameter could be directly defined and the second was given by the size-ratio of the used syringes. Beside this the size-ratio could only be chosen out of a small set of different syringes. This gave strong limitations to the verification of the experimental part. To give evidence for detailed aspects and to make general conclusions it is necessary to do measurements with equipment where all flow-parameters can be

defined and controlled independently. This will result in more detailed performance diagrams of the characterized devices.

- To push the limit of the focused sample dimensions it will be useful to analyse the characteristics of the pumps e.g. under the aspects of limitations of the pressure they can drive. Maybe it will be necessary to replace the pumps by a real pressure driven system like in [6] instead of a flow rate driven system.

- As experimental results by *Gabriel Hairer* show, who used the devices with a 200 μm thin covering glass, thinner covering glasses increase the optical resolution and the contrast of the confocal microscopic measurements a lot. The ideally thickness is of about 170 μm thickness. This thickness will allow the use of high power microscope objective lenses which are corrected to the standard cover slip of 170 μm.

6.2 Outlook

The different designs were chosen to give a lot of further applications to future analysis and experiments. For example, the device No. III will allow to reduce the lower limits for the achievable sample limits even further due to the smaller channel geometries. This is proven by the work of Gabriel Hairer, who used the device No. III to push these limits. Fabricating the wafers with an SU-8 layer of different thickness offers the opportunity to study the influence of the channel geometry on the shape of the sample flow more detailed. In the case of the non-coaxial devices additional masks can be designed and added to the process flow to integrate, for example a Coulter-counter (see [11]). The designs allow further studies of focusing and aligning sample streams within a microchannel. The next possible step could be to use the technique of coaxial sheath flows for the purpose to align asymmetric particles, e.g. long bacteria strings or proteins axial within the microchannel.

Chapter 7

Appendix

7.1 Lithographic Masks

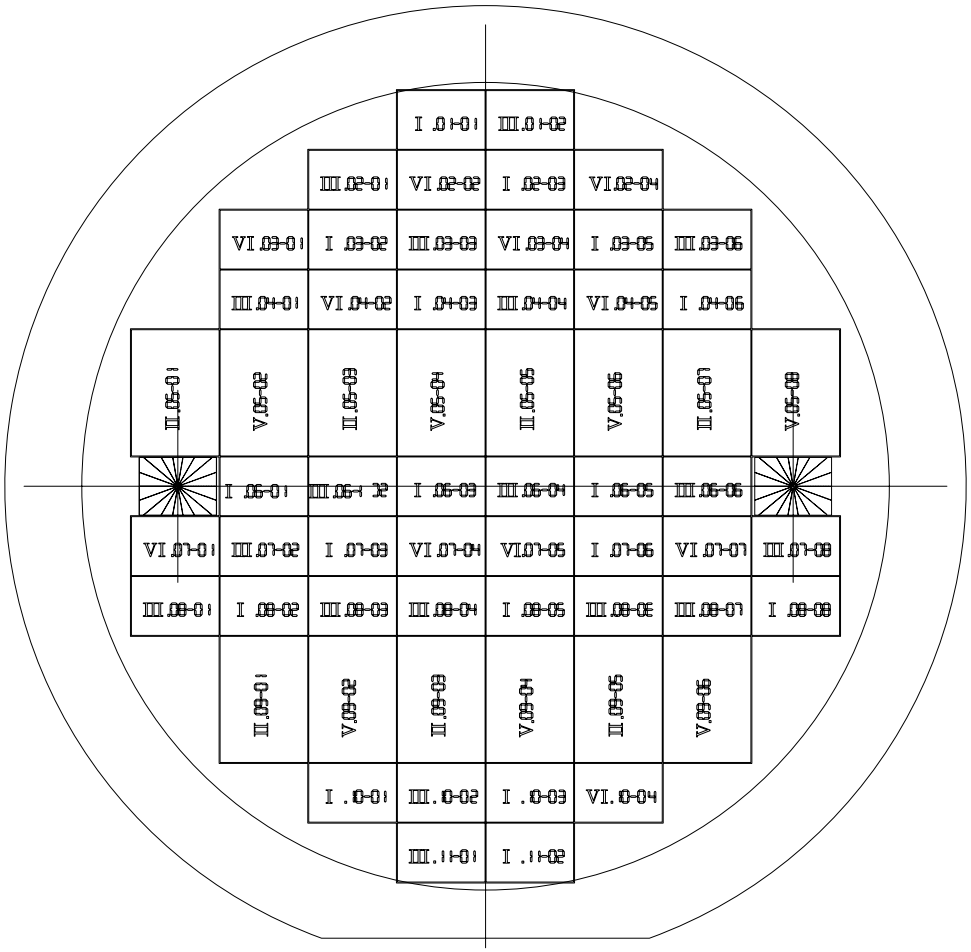

Figure 7.1: Position and arrangement of the different devices on the wafer surface. The index numbers refer to Table 4.1.

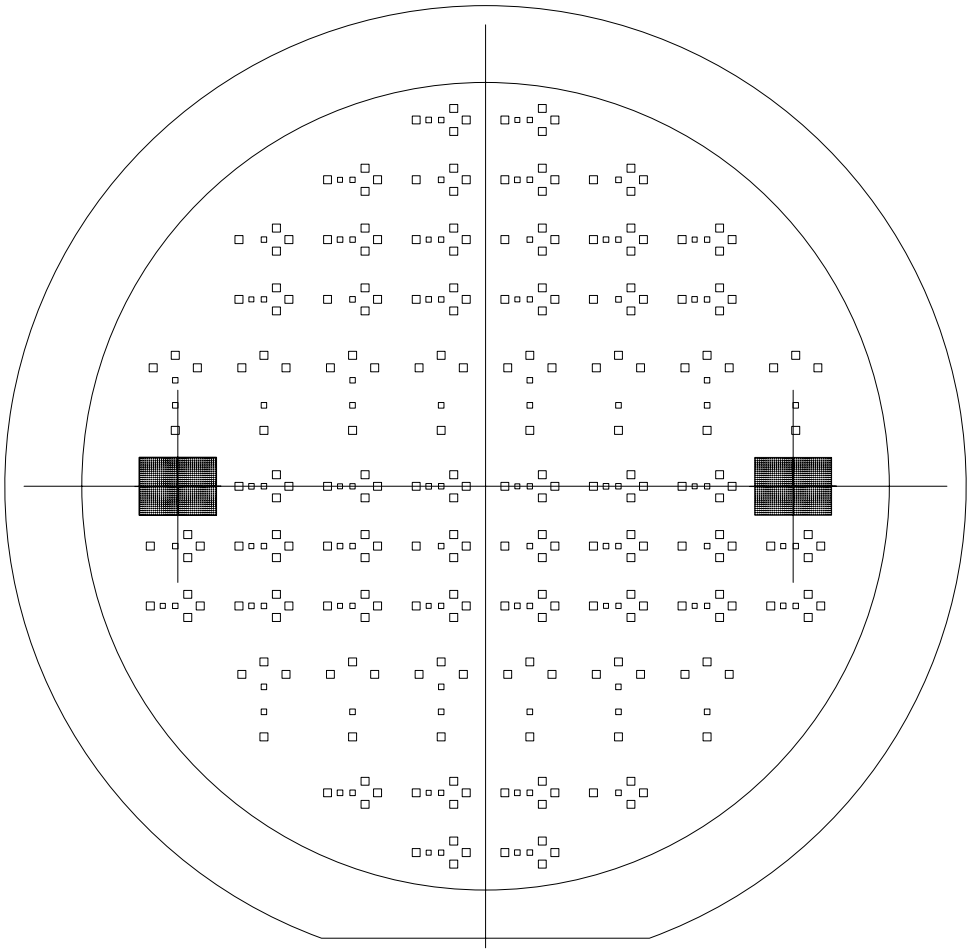

Figure 7.2: ACAD layout of the lithographic mask for etching the holes into the silicon wafer with KOH.

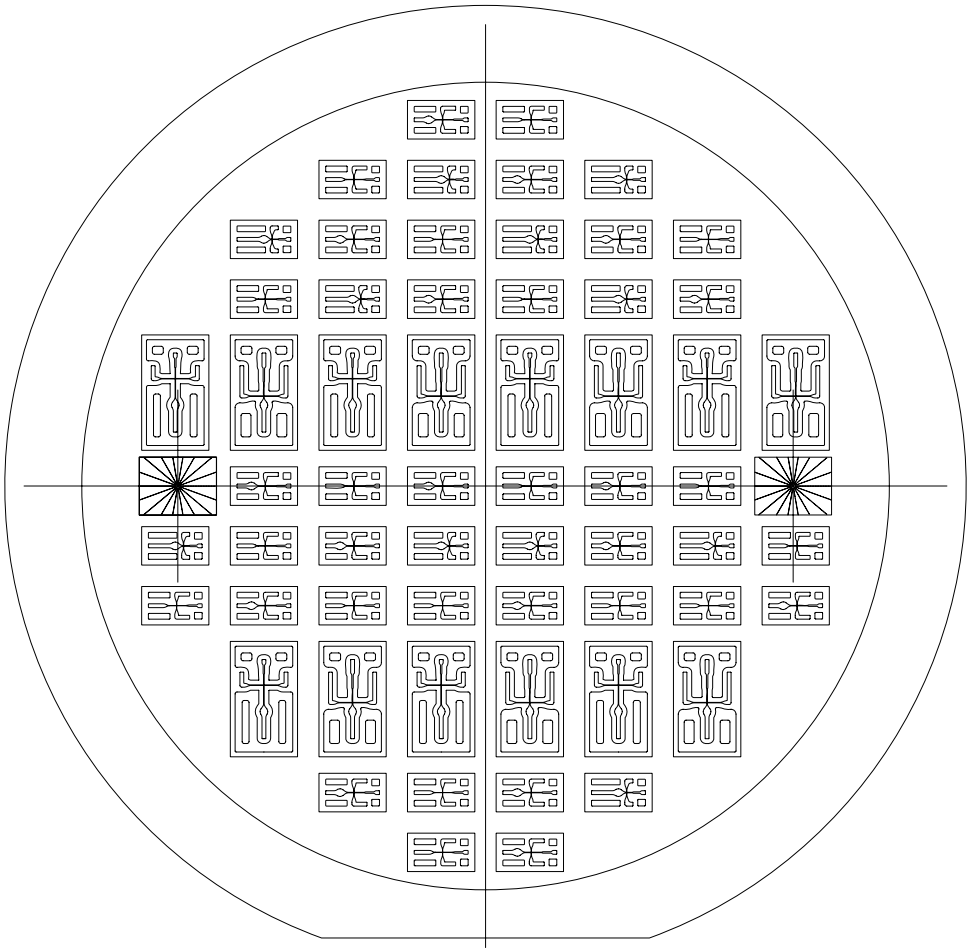

Figure 7.3: ACAD layout of the lithographic mask for the silver sacrificial layer.

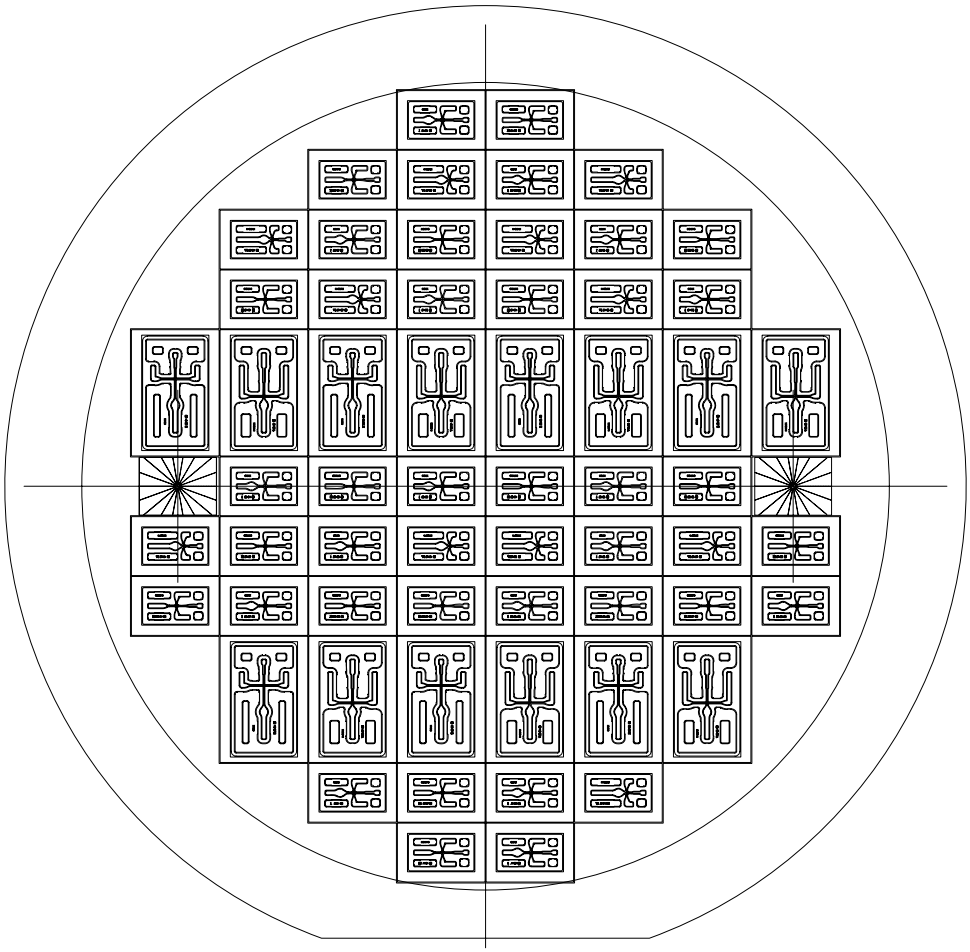

Figure 7.4: ACAD layout of the lithographic mask for defining the pattern of SU-8 on the glass wafer.

7.2 Technical Drawings

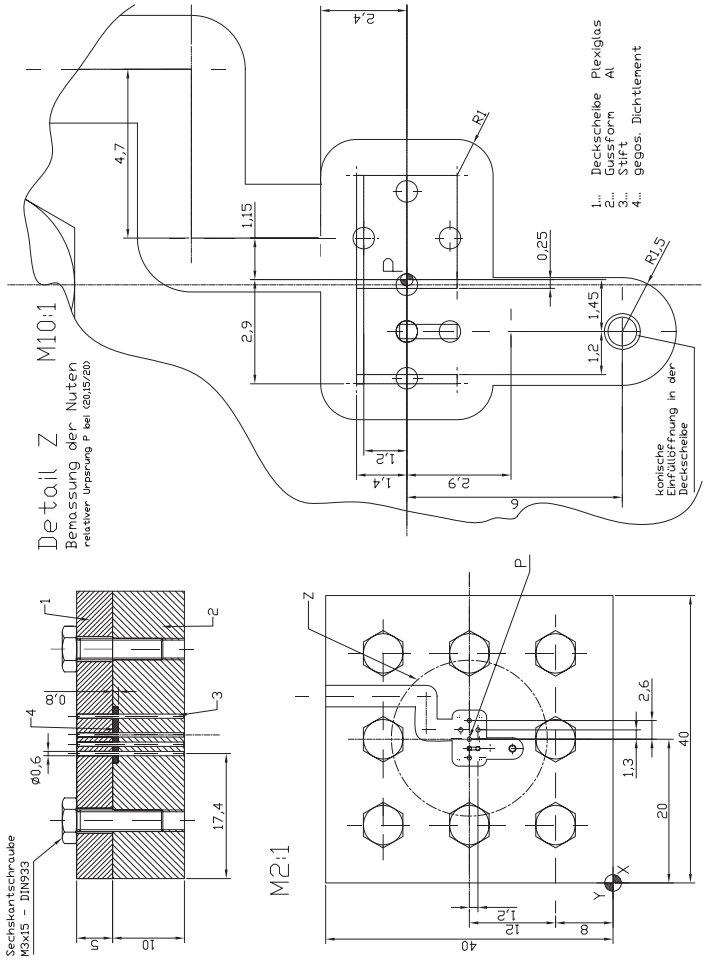

Figure 7.5: ACAD drawing for fabrication of the mould.

List of Figures

Bibliography

[1] J. H. Nieuwenhuis *et al.*, "Integrated flow-cells for novel adjustable sheath flows," *Lab Chip*, vol. 3, pp. 56–61, 2003.

[2] Z. Wu *et al.*, "Hydrodynamic focusing in microchannels under consideration of diffusive dispersion: Theories and experiments," *Sens. Actuators B*, vol. 107, pp. 965–974, 2005.

[3] G.-B. Lee *et al.*, "The hydrodynamic focusing effect inside rectangular microchannels," *J. Micromech. and Microeng.*, vol. 16, pp. 1024–1032, 2006.

[4] N. Sundarajan *et al.*, "Three-dimensional hydrodynamic focusing in polydimethylsiloxane (pdms) microchannels," *JMEMS*, vol. 13-4, pp. 9559–567, 2004.

[5] G. Hairer *et al.*, "Analysis of micrometer sample flows in a non coaxial sheath flow device," *Transducers 2007 and Eurosensors XXI (accepted for publication)*.

[6] J. B. Knight *et al.*, "Hydrodynamic focusing on a silicon chip: Mixing nanoliters in microseconds," *Physical Review Letters*, vol. 80, pp. 3863–3866, 1998.

[7] N.-T. Nguyen *et al.*, *Fundamentals and Applications of Microfluidics*, 1st ed. Norwood, MA02062, USA: Artech house, Inc., 2002.

[8] Fox and McDonald, *Introduction to Fluid Mechanics*. New York, USA: Wiley, 1999.

[9] P. A. Thompson *et al.*, "A general boundary condition for liquid flow at solid surfaces," *Nature*, vol. 389, pp. 360–362, 1997.

[10] J. Berthier and P. Silberzahn, *Microfluidics for Biotechnology*. Norwood, MA02062, USA: Artech house, Inc.

[11] S. Gawad *et al.*, "Micromachined impedance spectroscopy flow cytometer for cell analysis and particle sizing," *Lab Chip*, vol. 1, pp. 76–82, 2001.

[12] D. Huh *et al.*, "Microfluidics for flow cytometric analysis of cells and particles," *IOP Publishing Ltd.*, vol. 26, pp. R73–R98, 2005.

[13] R. Yang *et al.*, "Microfabrication and test of a three-dimensional polymer hydro-focusing unit for flow cytometry applications," *Sens. Actuators A*, vol. 118, pp. 259–267, 2005.

[14] G. Hairer *et al.*, "Experiments on hydrodynamic focusing of non coaxial sheath flows," *Proceedings of IEEE Sensors 2006*, pp. 431–434.

[15] (2007) The COMSOL website. [Online]. Available: http://www.comsol.com/

[16] A. Wolff *et al.*, "Integrating advanced functionality in a microfabricated high-throughput fluorescent-activated cell sorter," *Lab Chip*, vol. 3, pp. 22–27, 2003.

[17] S. Shoji *et al.*, "Design and fabrication of micromachined chemical/biochemical systems," *RIKEN Review*, vol. 36, pp. 8–11, 2001.

[18] P. Svasek *et al.*, "Fabrication of miniaturized fluidic devices using su-8 based on lithographic and low temperature wafer bonding," *Sens. Actuators A*, vol. 115, pp. 591–599, 2004.

[19] W. Wu *et al.*, "Mems-based flow cytometry: Microfluidics-based cell idendification system by fluorescent imaging," *26th Annual International Conference of the IEEE EMBS*, pp. 2579–2581, 2004.

[20] C. Simonnet *et al.*, "Two-dimensional hydrodynamic focusing in a simple microfluidic device," *Applied Physics Letters*, vol. 87, p. 114104, 2005.

[21] (2007) The Wikipedia website. [Online]. Available: http://www.wikipedia.com/